A DETERMINATION OF THE PERMANENT DIPOLE MOMENT OF HD: CORRECTION FOR INTRACOLLISIONAL INTERFERENCE

A Thesis

Submitted to

the Faculty of Graduate Studies

University of Manitoba

In Partial Fulfillment

of the Requirements for the Degree

Master of Science

by

J. Bradley Nelson

May 1982

A DETERMINATION OF THE PERMANENT DIPOLE MOMENT OF HD: CORRECTION FOR INTRACOLLISIONAL INTERFERENCE

BY

J. BRADLEY NELSON

A thesis submitted to the Faculty of Graduate Studies of the University of Manitoba in partial fulfillment of the requirements of the degree of

MASTER OF SCIENCE

ACKNOWLEDGEMENTS

I gratefully acknowledge Dr. George C. Tabisz for his invaluable aid and insight into this project. I would also like to especially thank Dr. Murray Neuman for the many conversations and the time spent helping me throughout the last three years. Finally, I would like to thank Ray and Vivek for their friendship and comaraderie within, and outside of, the lab.

ABSTRACT

Initial attempts to measure the permanent dipole moment of HD gas by absorption spectroscopy neglected interference effects between the permanent and collision-induced moments of the gas molecules. The far-IR spectrum of HD as a function of density has been obtained with a modified Michelson interferometer at a spectral resolution of 1 cm^{-1}. Extrapolating back to "zero density" yielded, for the ground vibrational state, a J-dependent dipole moment ranging in magnitude between 8.0 and 9.8 x 10^{-4} Debye. A J-dependent intracollisional interference parameter "a" was measured and found to be between -5.5 ± 1.3 and $-9.6 \pm .5 \times 10^{-3}$ $Amagat^{-1}$. These are in excellent agreement with calculations [1], [2], [3] indicating $|\mu_o| = 8.4 \times 10^{-4}$ Debye and [4] $|a| = 5.4 \times 10^{-3}$ $Amagat^{-1}$.

[1] Wolniewicz L.; Can. J. Phys. 54, 672 (1976).

[2] Ford L. and Browne J.; Phys. Rev. A. 16, 1992 (1977).

[3] Bunker P.; J. Mol. Spec. 46, 119 (1973).

[4] Tipping R. H., Poll J.D. and McKellar A. R. W.; Can. Jour. Phys. 56, 75 (1978).

TABLE OF CONTENTS

LIST OF FIGURES

LIST OF TABLES

INTRODUCTION

Hydrogen molecules (H_2) do not possess a permanent dipole moment between vibrational states because of mass and charge symmetries. The center of mass is at the center of charge in the "stationary" molecule.

By the symmetry of the nuclei, the surrounding electron cloud must also be symmetric about the center of mass. As the molecule oscillates, the electron cloud of each atom will be forced to follow the motion of its governing nucleus. Even if the electron cloud lags behind its nuclear counterpart (due to inertia), the total electron configuration remains symmetric about the same point as the two positive charges do. Thus in the classical approach, we do not expect hydrogen molecules to possess a permanent dipole moment.

Hydrogen deuteride (HD), however, has a mass asymmetry. As the molecule oscillates, the hydrogen nucleus moves much further (relatively) than the deuterium nucleus does. In the event of Born-Oppenheimer breakdown (electronic and nuclear motions are coupled), the total electron configuration will not be symmetric about the same point as the two positive charges will be. Classically then we might expect HD to exhibit a dipole moment between vibrational states.

Calculations by Wolniewicz [1] and [2], Ford and Browne [3], Bunker [4], Kolos and Wolniewicz [5] and [6] indicate there should be a dipole moment between rotational states as well. Our experiments measured the dipole moment of HD in the ground vibrational state.

At sufficiently high pressures (> 10 atmospheres) short lifetime

collision-induced dipole moments arise. The total dipole moment is then the sum of the permanent and induced moments. Because the absorption by a molecule is proportional to the square of the dipole moment, three terms appear in the total absorption. The first is due solely to the permanent moment and gives rise to sharp spectral features. The second term is purely collision-induced, yielding a broad band background absorption. The third is a cross-term between the permanent and induced dipole moments. Its dependence on the permanent moment ensures that it too gives rise to sharp spectral lines [7]. Depending on the signs of the two components, this cross term may enhance or reduce the sharp spectral peaks. The intracollisional interference parameter is an estimate of the relative magnitudes and signs of the collision-induced and permanent dipole moments.

Experiments in 1968 by Trefler and Gush [8] and later by McKellar [9], designed to find the permanent dipole moment of HD neglected this interference effect. Gush's measured values were almost 40% lower than the best theoretical values for the ground vibrational state permanent dipole moment.

Our experiments were designed to include the intracollisional interference effects, in hopes of rectifying the discrepancy between measured and calculated values of $|\mu_o|$.

CHAPTER 1

CALCULATIONS OF THE DIPOLE MOMENT OF HD

The first quantum approach to calculating the permanent dipole of HD was attempted by Wick [10] in 1935. Using the first order perturbation theory applied to the hydrogen molecule, he calculated a dipole moment between oscillator states in good agreement with later measurements.

FIGURE 1. THE HYDROGEN DEUTERIDE MOLECULE

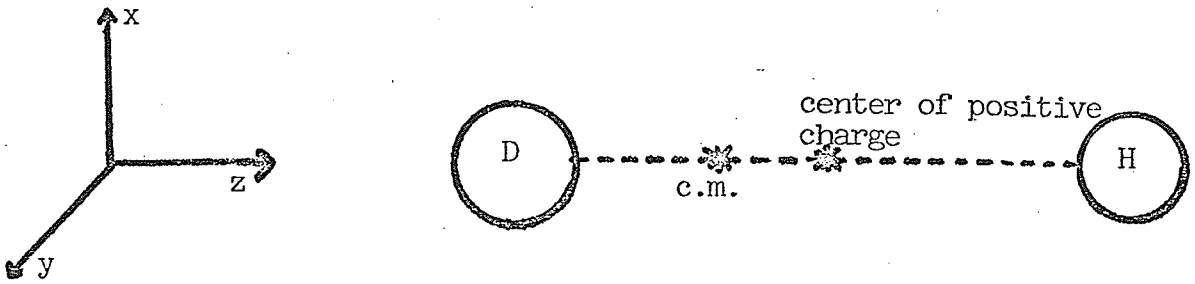

For the remainder of this thesis, we shall consider the direction from D to H as a positive direction. i.e. if $\vec{\mu}$ is negative, it implies that the dipole moment points from the hydrogen to the deuterium nucleus.

For the dipole moment along the internuclear (z) axis, we

write

$$\vec{\mu}_z = e\vec{z} \,, \tag{1.1}$$

where

$\vec{\mu}_z$ is the dipole moment operator

e is the electron charge

and $\vec{z} = \vec{z}_1 + \vec{z}_2$.

We shall adopt the convention of upper case letters to denote nuclear coordinates and lower case letters to denote electronic coordinates. Thus the deuterium nucleus is at the point (X_1, Y_1, Z_1) while its electron is at (x_1, y_1, z_1), (relative to the deuterium nucleus). The subscript 2 refers to the hydrogen nucleus.

From Kolos and Wolniewicz [7], we can write the Hamiltonian for a two electron diatomic molecule as

$$H = H_o + H' \tag{1.2}$$

where

$$H_o = H_{e\ell} - \frac{\hbar^2}{2\mu} \nabla_R - \frac{\hbar^2}{8\mu} (\nabla_{z_1} + \nabla_{z_2})^2 \tag{1.3a}$$

and

$$H' = -\frac{\hbar^2}{2\mu_a} \nabla_R \, (\nabla_{z_1} + \nabla_{z_2}) . \tag{1.3b}$$

Also,

$H_{e\ell}$ is the clamped nuclei Hamiltonian

∇_R is the gradient with respect to nuclear coordinate

∇_{z_1} is the gradient with respect to electronic coordinates for the first atom

μ is the reduced mass

$$= \frac{M_H M_D}{M_H + M_D} = \frac{2}{3} M_H$$

and

$$\mu_a = \frac{M_H M_D}{M_H - M_D} = -2 M_H .$$

Thus the perturbation energy of the internuclear potential H' can be expressed as

$$H' = + \frac{\hbar^2}{4M_H} \nabla_R [\nabla_{z_1} + \nabla_{z_2}] .$$

Notice for the case of pure hydrogen all the terms in H_o are retained. However $1/\mu_a = 0$, so H' equals zero.

In the adiabatic approximation, the nuclear and electronic motions are separable. Thus we can re-define the perturbation energy as a product of two commuting operators

$$H' = \lambda(R)\, \Gamma(r) = \Gamma(r)\, \lambda(R)$$

where

$$\lambda = + \frac{\hbar^2}{4M_H} \nabla_R \tag{1.4}$$

and

$$\Gamma = \nabla_{z_1} + \nabla_{z_2} . \tag{1.5}$$

From second order perturbation theory [10], [11], we can express the dipole moment between two states in the following way

$$\langle a|\mu_z|c\rangle = -e \sum_b \left(\frac{\langle a|z|b\rangle\langle b|H'|c\rangle}{E(c) - E(b)} + \frac{\langle a|H'|b\rangle\langle b|z|c\rangle}{E(a) - E(b)} \right) . \tag{1.6}$$

Here

$\langle a|z|b\rangle = \langle a|z_1+z_2|b\rangle$ is the matrix element of the operator z between states $|a\rangle$ and $|b\rangle$,

$\langle a|H'|b\rangle$ is the matrix element of the operator H' between these same states

and

E(a) is the energy of the molecule in state $|a\rangle$.

Note that $|a\rangle$ and $|c\rangle$ are the initial and final states respectively while $|b\rangle$ is any allowed intermediate state.

Alternatively we can write, as before

$$\begin{aligned} \langle a|H'|b\rangle &= \langle a|\lambda\Gamma|b\rangle \\ &= \sum_d \langle a|\lambda|d\rangle\langle d|\Gamma|b\rangle \end{aligned} \tag{1.7}$$

because $\sum_d |d\rangle\langle d|$ is just the identity operator.

If we assume the form of H', the perturbation component of the internuclear potential, to be that of a harmonic oscillator in one dimension, then we can find alternate expressions for both $\langle\alpha|\lambda|\beta\rangle$ and $\langle\alpha|\Gamma|\beta\rangle$.

Following the notation of Böhm [12]

$$H_{\text{harmonic osc.}} = \frac{P^2}{2\mu} + \frac{\mu\omega^2}{2} Q^2 .$$

Here P is the quantum mechanical momentum operator

Q is the quantum mechanical displacement operator

and μ,ω are system constants.

$$\therefore \quad [H, Q] = HQ - QH$$

$$= [\frac{P^2}{2\mu} + \frac{\mu\omega^2}{2} Q^2, Q]$$

$$= (1/2\mu)[P^2, Q]$$

$$= (1/\mu) P[P, Q]$$

$$= - \frac{i\hbar P}{\mu} \quad .$$

$$\therefore \quad P = \frac{i\mu}{\hbar} (HQ - QH) \quad .$$

Taking this operator between the states $|\alpha\rangle$ and $|\beta\rangle$ yields

$$\langle\alpha|P|\beta\rangle = \frac{i\mu}{\hbar} \langle\alpha|HQ-QH|\beta\rangle$$

$$= \frac{i\mu}{\hbar} [E(\alpha) - E(\beta)] \langle\alpha|Q|\beta\rangle \quad .$$

Identifying P with $(\hbar/i)(\nabla_{z_1} + \nabla_{z_2})$ and Q with $z = z_1 + z_2$, then we have immediately

$$\langle\alpha|\Gamma|\beta\rangle = \frac{m_e}{\hbar^2} [E(\alpha) - E(\beta)] \langle\alpha|z|\beta\rangle \qquad (1.8)$$

because in this case the reduced mass μ is just the electron mass m_e.

Similarly if we identify P with $(\hbar/i)\nabla_R$ and Q with the internuclear coordinate R, then we get

$$\langle\alpha|\frac{\hbar}{i} \nabla_R|\beta\rangle = \frac{i\mu}{\hbar} \langle\alpha|HR - RH|\beta\rangle$$

$$= \frac{i\mu}{\hbar} [E(\alpha) - E(\beta)] \langle\alpha|R|\beta\rangle \quad .$$

Multiplying both sides by $\frac{\hbar}{-i4M_H}$ gives us the operator λ between the states $|\alpha\rangle$ and $|\beta\rangle$.

$$\langle\alpha|\lambda|\beta\rangle = \frac{1}{6}\,[E(\alpha) - E(\beta)]\ \langle\alpha|R|\beta\rangle \tag{1.9}$$

because in this case the reduced mass is equal to 2/3 of the proton mass M_H.

Using (1.8), we rewrite (1.6) as

$$\mu_z(a,c) = -\frac{eM_e}{\hbar^2} \sum_{bd} \frac{z(a,b)\ z(b,d)\ [E(d) - E(b)]\ \lambda(d,c)}{E(c) - E(b)} + \frac{\lambda(a,d)\ [E(b) - E(d)]\ z(d,b)\ z(b,c)}{E(a) - E(b)} \tag{1.10}$$

where for ease of inspection we've written $\langle\alpha|X|\beta\rangle$ as $X(\alpha,\beta)$. Rewriting the energy difference terms as

$$E(d) - E(b) = E(d) - E(c) + E(c) - E(b)$$

and

$$E(b) - E(d) = E(b) - E(a) + E(a) - E(d)$$

gives us

$$\mu_z(a,c) = -\frac{eM_e}{\hbar^2} \sum_{bd} z(a,b)\ z(b,d)\ \lambda(d,c)\ \left[1 + \frac{E(d) - E(c)}{E(c) - E(b)}\right] + \lambda(a,d)\ z(d,b)\ z(b,c)\ \left[1 + \frac{E(a) - E(d)}{E(a) - E(b)}\right].$$

The first and third terms cancel for the following

reason:

$$\sum_b |b\rangle\langle b| = I = \sum_d |d\rangle\langle d|$$

$$\therefore \quad \sum_{b,d} \langle a|z|b\rangle\langle b|z|d\rangle\langle d|\lambda|c\rangle$$

$$- \langle a|\lambda|d\rangle\langle d|z|b\rangle\langle b|z|c\rangle$$

$$= \langle a|zz\lambda - \lambda zz|c\rangle$$

$$= 0$$

because λ is not a function of z. Thus we arrive at the equation for μ_z between the states (a) and $|c\rangle$

$$\mu_z(a,c) = -\frac{em_e}{\hbar^2} \sum_{b,d} \frac{[E(d)-E(c)]}{E(c)-E(b)} z(a,b)\ z(b,d)\ \lambda(d,c) + \frac{[E(a)-E(d)]}{E(a)-E(b)} \lambda(a,b)\ z(d,b)\ z(b,c). \tag{1.11}$$

Using 1.9 for $\lambda(a,d)$ and $E(\alpha) - E(\beta) = \hbar\,\omega(\alpha,\beta)$ in the numerator, (1.11) becomes:

$$\mu_z(a,c) = +\frac{em_e}{6} \sum_{b,d} \frac{z(a,b)\ z(b,d)}{E(c) - E(b)}\ \omega^2(d,c)\ R(d,c) + \frac{z(d,b)\ z(b,c)\ \omega^2(a,d)}{E(a) - E(b)}\ R(a,d), \tag{1.12}$$

The polarizability in a state $|a\rangle$ is defined [10] as:

$$\alpha_a = -2e^2 \sum_b \frac{z(a,b)\ z(b,a)}{E(a) - E(b)} .$$

Similarly $$\alpha_c = -2e^2 \sum_b \frac{z(c,b)\ z(b,c)}{E(c) - E(b)} .$$

If in the first term in (1.12), we make the following assumptions:

$$\left.\begin{array}{ll} (1) & |d\rangle = |a\rangle \\ (2) & |a\rangle = |ov\rangle \\ & |c\rangle = |ov'\rangle \end{array}\right\} \text{ground electronic state, different vibrational states.}$$

$\therefore$ $E(c) \approx E(a)$ and the first term in (1.12) is approximately:

$$\approx 2/3\ e^2 m_e \sum_b \frac{z(a,b)\ z(b,a)}{E(a) - E(b)}\ \omega^2_{(v,v')}\ R(v,v')$$

$$\approx -\frac{m_e}{3e}\ \omega^2_{(v,v')}\ \alpha_v\ R(v,v').$$

Similarly for the second term, we assume

$$\left.\begin{array}{ll} (1) & |c\rangle = |d\rangle \\ (2) & |a\rangle = |ov\rangle \\ & |c\rangle = |ov'\rangle \end{array}\right\} \text{i.e. ground electronic state, different vibrational state.}$$

$\therefore$ $E(c) \approx E(a)$ and the second term becomes

$$\approx -\frac{m_e}{3e}\ \omega^2_{(v,v')}\ R(v,v')\ \alpha_{v'}.$$

Thus $\mu_z(a,c) = -\frac{2}{3e}\ m_e\ \omega^2_{(v,v')}\ [\frac{\alpha_v + \alpha_{v'}}{2}]\ R(v,v')$

or

$$\mu_z(a,c) = -\frac{2}{3e}\ m_e\ \omega^2_{(v,v')}\ (\alpha_{ave})\ R(v,v'). \qquad (1.13)$$

To evaluate this expression, we assume that R is the quantum mechanical nuclear displacement. Following the treatment of Böhm [12]

$R(v,v') = \langle v|R|v'\rangle$. However $R = \sqrt{\frac{\hbar}{2\mu\omega}}(a + a^+)$ where a and a^+ are the lowering and raising operators respectively. Again μ is the reduced mass and ω is a transition frequency to be determined later.

$$\therefore \quad R|v'\rangle = \sqrt{\frac{\hbar}{2\mu\omega}}\left[\sqrt{v'}\,|v'-1\rangle + \sqrt{v'+1}\,|v'+1\rangle\right]$$

$$\text{or} \quad \langle v|R|v'\rangle = \sqrt{\frac{\hbar}{2\mu\omega}}\left[\sqrt{v'}\,\langle v|v'-1\rangle + \sqrt{v'+1}\,\langle v|v'+1\rangle\right].$$

For the fundamental band, i.e. $|v'\rangle = |01\rangle$ and $|v\rangle = |00\rangle$, we get

$$R_{00\to01} = \sqrt{\frac{\hbar}{2\mu\omega}}(1).$$

From Raman studies it has been found [13] that $\omega \approx 3800$ cm^{-1} so that $R_{00\to01} \approx 8 \times 10^{-13}$ meters.

The polarizability of HD is a function principally of electronic structure and thus should be equal to that of H_2. From [14] we find

$$\alpha_{H_2} \approx 10^{-40} \quad \text{in MKS units}$$

which gives a value of the dipole moment of

$$|\mu_z| \sim 3 \times 10^{-34} \quad \text{Coulomb meters}$$
$$\sim 1 \times 10^{-4} \quad \text{Debye.}$$

The model yielded a reasonable value for the fundamental band (vs. the experimental value of $|\mu_z| \approx .6 \times 10^{-4}$ Debye from McKellar [9]), but, because of the harmonic oscillator approximation, it predicted no dipole moment for ground state rotational transitions.

i.e. $\langle 0j|R|0j'\rangle = 0 \qquad (\Delta v = 0)$.

Similarly it predicted no overtone bands ($\Delta v = 2, 3, 4 \ldots$).

Wu [15] improved upon the model of Wick by considering a Morse potential to calculate R(v, v'). This potential has the form [16] (see Figure 2)

$$V(R) = V_o[1 - e^{-aR}]^2 - V_o$$

where V_o is the minimum of the harmonic oscillator potential, R is the internuclear distance and "a" is a damping constant.

Using this model, Wu found an expression for R(v, v') [15]

$$R(v, v') = \frac{A}{[1 - (v+v'+1)\,\chi_e][v-v']} \cdot \left[\frac{v![1 - (2v'+1)\chi_e][1 - (2v+1)\,\chi_e]}{v'![1 - (v'+1)\,\chi_e]\ldots[1 - v\chi_e]}\right] \cdot \chi_e^{\left(\frac{v-v'-1}{2}\right)} .$$

Here $$A = \left[\frac{3\hbar}{8M_H}\,\omega(v, v')\right]^{\frac{1}{2}}$$

$$\chi_e = \frac{\omega}{4D} = 0.026 \quad \text{for HD}$$

ω is the vibrational frequency

and D is the dissociation energy.

This model predicted a value of the dipole moment for the fundamental band of $\sim 10^{-4}$ Debye and allowed the harmonics of that band.

FIGURE 2 THE MORSE POTENTIAL

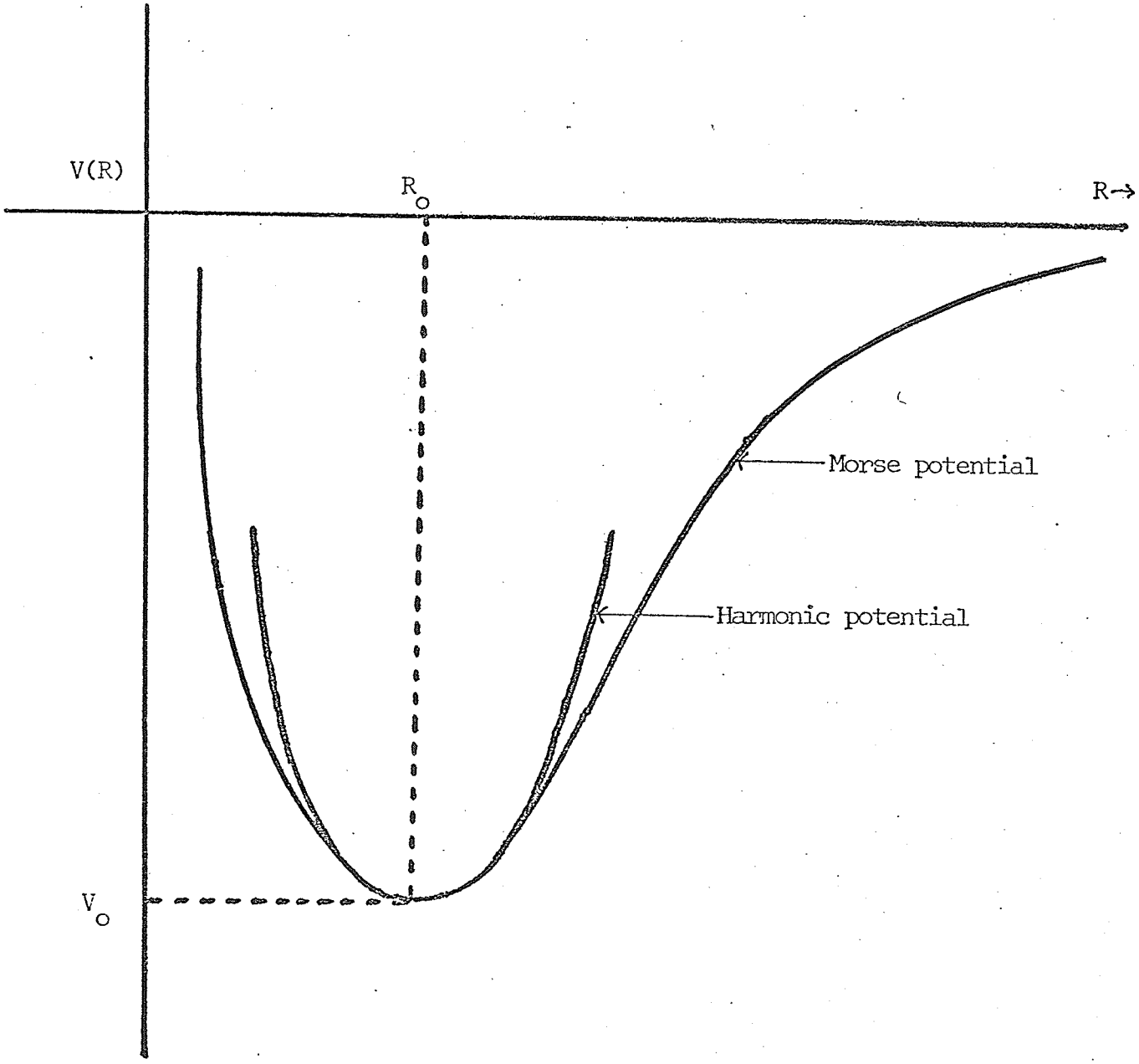

i. e. the transitions $\langle 01|\mu_z|00\rangle$, $\langle 02|\mu_z|00\rangle$, $\langle 03|\mu_z|00\rangle$ etc. were predicted with the ratios of intensities corresponding closely to the values measured by Herzberg [17].

Wu however did not predict any rotational spectrum in the ground vibrational state, again because of his choice of internuclear potential.

Blinder [18] used a slightly different approximation than either Wu or Wick. He started from eq. (1.11) derived by Wick:

$$\mu_z(a,c) = -\frac{em_e}{\hbar^2} \sum_{b,d} \left[\frac{E(d)-E(c)}{E(c)-E(b)}\right] z(a,b)\, z(b,d)\, \lambda(d,c)$$

$$+ \frac{[E(a)-E(d)]}{E(a)-E(b)}\, \lambda(a,d)\, z(d,b)\, z(b,c).$$

However $[E(a)-E(d)]\,\lambda(a,d) = \langle a|(E(a)-E(d))\lambda|d\rangle$

$= \langle a|[H,\lambda]|d\rangle$

where $H|a\rangle = E|a\rangle$.

He re-defined the total Hamiltonian as:

$$H = H_{\text{electronic}}(z_1 z_2) + V(R) + Q(R, z_1, z_2)$$

where $H_{\text{electronic}}(z_1, z_2)$ takes account of all purely electronic interactions, $V(R)$ is an internuclear potential and $Q(R, z_1, z_2)$ is a small cross term.

Then $[H,\lambda] \simeq \frac{\partial V(R)}{\partial R}$.

Defining a new operator $W = z\,\frac{\partial V(R)}{\partial R}$, and assuming only the first state

in the sums over b and d is important, Blinder found

$$\mu_z(a,c) = -\frac{em_e}{h^2}\left[\frac{z(a,1)W(1,c)}{E(c)-E(1)} + \frac{W(a,1)z(1,c)}{E(a)-E(1)}\right].$$

For the ground vibrational state, this reduced to

$$\mu_z(j',j) = +\frac{em_e}{h^2}\,\langle 0j'|zW|0j\rangle\,\frac{1}{E(1)-E(0)}$$

where j and j' refer to the rotational quantum numbers of the initial and final states.

To calculate the matrix elements in the above expression, Blinder evaluated the function zW in the ground electronic state for several representative values of R. Fitting a polynomial to a plot of these points yielded an approximate analytic form for $\mu_z(R)$. Integrating this over the ground vibrational Morse eigenfunctions, i.e.

$$\langle 0j'|\mu_z(R)|0j\rangle = \int_{-\infty}^{+\infty} \psi^{\dagger}_{0j'}\,\mu_Z(R)\,\psi_{0j}\,d\tau$$

yielded $\mu_z(0j',0j) \approx -8.89 \times 10^{-4}$ Debye.

In a subsequent paper [19], Blinder disregarded the assumption that only the first state contributed to the sum. Following the same derivation, the calculated; $\mu_z(0j',0j) = -5.67 \times 10^{-4}$ Debye.

Bunker [4] re-defined the perturbation component in the total Hamiltonian as a sum of 3 terms:

$$H' = H'_{rot} + H'_{vib} + H'_{elec}.$$

Here H'_{elec} mixes electronic states with $\Delta n = 1$ and H'_{vib}, H_{rot} mix states of the same electronic level. Each of these three terms gives rise to an independent component of the permanent dipole moment, the

sum of which is the total permanent dipole moment. Explicit forms are given as [4]:

$$\mu_{rot}(v'j',vj) = \frac{em_e}{\mu_a} \langle v'j|1/R\ \langle 0|\left(\sum_i x_i\right)^2|0\rangle|vj\rangle$$

where x_i are the electronic coordinates in the molecule fixed reference frame and $\mu_{vib}(v'j',vj) = \left\langle v'j'\right| - \frac{em_e}{2\mu_a} \nabla_R \left(\langle 0j'|z^2|0j\rangle\right)\left|vj\right\rangle$

$$- \frac{\pi^2 m_e}{3e} \sum_{\bar{v}} \omega^2(\bar{v},v)\ [\alpha(v',\bar{v})\ R(\bar{v},v) + R(v',\bar{v})\alpha(\bar{v},v)]$$

Note that the second term is just that derived by Wick and Wu.

To evaluate μ_{rot}, Bunker used the value for $\langle 00|z^2|00\rangle$, calculated by Kolos and Wolniewicz [6], of -0.198 Å. Thus to a good approximation, Bunker found:

$$\mu_{rot}\ (0,0) \approx \frac{2em_e}{\mu_a R_e}\ (-.198)$$

$$\approx + 7.0 \times 10^{-4} \text{ Debye} .$$

Taking the derived value for $\mu_{elec} + \mu_{vib}$ from Kolos and Wolniewicz [6] of:

$$\mu_{elec}(0j',0j) + \mu_{vib}(0j',0j) = - 15.4 \times 10^{-4} \text{ Debye},$$

Bunker found $\mu(0j',0j) = - 8.4 \times 10^{-4}$ D.

Wolniewicz [1], [2] constructed wave functions using a variational technique. He used the following expansion for the wavefunction ψ

$$\psi_{J,0} \simeq 2\{x_1 B_1 + x_2 B_2\}\, d_{o,1}^{J}(\theta)$$

where x_i is the coordinate along the x axis of the i'th electron in the molecule fixed frame, B_i are functions to be optimized later and $d_{o,1}^{J}$ is a function containing angular components of ψ. He chose the form of B_i to be a 180 term expansion consisting of 20 electronic terms and hermite polynomials up to order 9. Integrating the dipole operator over these wave function yielded transition matrix elements.

In the perturbation expansion there is a sum over states of matrix elements giving the total dipole moment. Summing over only the Π_μ states, the total dipole moment was found to be -15.4×10^{-4} D [2] while summing over both the Π_μ and Σ_g symmetric states yielded a permanent dipole moment of -8.4×10^{-4} D [1]. Wolniewicz found a slight J-dependence but only in the 3rd significant figure (see Table 5 Ch. 7).

The most recent calculations were performed by Ford and Browne [3]. They used an instantaneous dipole moment function D(R) whose matrix element was taken between initial and final state vibrational wave functions.

They expressed the wavefunctions as

$$\psi_{J\Lambda m} = \left(\frac{2J+1}{8\pi^2}\right)^{\frac{1}{2}} D^J_{m\Lambda}(\phi,\Theta,\Psi)$$

where $D^J_{m\Lambda}(\phi,\Theta,\Psi)$ is a rotation matrix as defined by Rose [20] . Together with the equation for the perpendicular component of $\vec{\mu}$

$$\langle a|\mu_\perp|b\rangle \quad \sum_N \left(\frac{\langle a|\vec{r}_\perp|N\rangle\langle N|H'|b\rangle}{E(b)-E(N)} + \frac{\langle a|H'|N\rangle\langle N|\vec{r}_\perp|b\rangle}{E(a)-E(N)} \right) \tag{1.14}$$

where H' is as previously defined in (1.3b) and $\vec{r}_\perp$ is the component of $\vec{r}$ perpendicular to the internuclear axis, [whereas Wick used $\vec{\mu}_z = e\vec{z}$, $\vec{z} = \vec{z}_1+\vec{z}_2$, Ford and Browne used $\vec{\mu} = e\vec{r}$, $\vec{r} = \vec{r}_1+\vec{r}_2$] . Ford and Browne found

$$\langle a|\mu_\perp|b\rangle = (J+1)\langle a|D_\perp|b\rangle$$

$$= (J+1)\frac{1}{\mu_a}\langle a|\langle\psi_o|(r_\perp^2)|\psi_o\rangle|b\rangle .$$

Here $|\psi_o\rangle$ is the ground electronic state. To find $\langle a|\mu_{||}|b\rangle$, they used a sum over states equation similar to (1.14) with $\vec{r}_{||} = \vec{z}_1+\vec{z}_2$. This yielded

$$\langle a|\mu_{||}|b\rangle = (J+1)\frac{1}{\mu_a}\langle a|\langle\psi_o|(r_{||})^2|\psi_o\rangle|b\rangle .$$

Adding the two components together, they calculated a permanent dipole moment for HD in the ground vibrational state of -8.3×10^{-4} Debye. They too found a very slight J dependence (see Table 5, Chapter 7). The following table summarizes the calculations of the dipole moment of HD over the last 40 years.

Table 1. CALCULATED TRANSITION AND PERMANENT DIPOLE MOMENTS IN HD

Wick	1935	t*	1×10^{-4} D	Harmonic oscillator approximation only for $\Delta v = 1$.
Wu	1952	t	1×10^{-4} D	Used Morse potential to get overtone bands in ≈ correct ratios.
Blinder	1960	p	-8.89×10^{-4} D	First calculation for ground vibrational state. Used simple wave functions and summed over 1st excited level.
Blinder	1961	p	-5.67×10^{-4} D	First calculation for ground vibrational state. Used simple wave functions and summed over all excited levels.
Bunker	1973	p	-8.4×10^{-4} D	Found $\mu_{vib} + \mu_{rot} + \mu_{el} = \mu_{tot}$.
Wolniewicz	1976	p	-8.4×10^{-4} D	Variational method summed over states of u and g symmetries.
Ford and Browne	1977	p	-8.3×10^{-4} D	Used an instantaneous dipole moment function D(R) evaluated between initial and final state wavefunction.

* t refers to transition moments for the fundamental band.
p refers to the permanent moment for the ground vibrational state.

CHAPTER 2

DIPOLE STRENGTH VS. INTEGRATED ABSORPTION

The integrated absorption is related to the dipole moment by the following eqn. [8]

$$\int \frac{\alpha(\omega)}{\omega} d\omega = \frac{8\pi^3}{3ch} \frac{N_o}{Q} \left[e^{-\frac{E_i}{KT}} - e^{-\frac{E_f}{KT}}\right] (J+1) \left|p^A_{if}\right|^2 \quad (2.1)$$

where α - is the absorption coefficient

ω - is the central frequency of a given line

N_o - is Loschmidt's number

Q - is the state sum

E_i - is the energy of the initial state

E_f - is the energy of the final state

J - is the rotational quantum number of the initial state

and p^A_{if} - is the reduced matrix element of the allowed dipole moment.

We shall now give a derivation of this equation.

Einstein postulated that the probability of absorption per unit time is given by [21]

$$P_{if} = P B_{if} \quad (2.2)$$

where

P_{if} is the probability of absorption per unit time.

P is the radiation density as found by Planck

and

B_{if} is the Einstein coefficient of absorption.

Similarly

$$P_{fi} = A_{fi} + P\,B_{fi} \tag{2.3}$$

where

P_{fi} is the probability of emission per unit time

A_{fi} is the coefficient of spontaneous emission

and

B_{fi} is the coefficient of stimulated emission.

If we denote the number of atoms in state "α" by N_α, then in equilibrium the number of transitions between the two states per unit time are equal, and we can write

$$N_i\,P_{if} = N_f\,P_{fi}$$

$$\therefore \quad N_i\,B_{if}\,P = N_f\,[A_{fi} + P\,B_{fi}]$$

Thus

$$\frac{N_i}{N_f} = \frac{[A_{fi} + P\,B_{fi}]}{P\,B_{if}} \tag{2.4}$$

In equilibrium, however, the Boltzmann law applies and we write alternatively

$$\frac{N_i}{N_f} = e^{\frac{h\nu_{if}}{KT}} \tag{2.5}$$

Combining (2.4) and (2.5), and solving for P yields

$$P = \frac{A_{fi}}{(B_{if})(e^{\frac{h\nu_{if}}{KT}}) - B_{fi}} \tag{2.6}$$

From Planck's law, the radiation density is given by

$$P = \frac{8\pi h\nu_{if}^3}{c^3}\left[\frac{1}{e^{\frac{h\nu_{if}}{KT}} - 1}\right] \tag{2.7}$$

Equating (2.6) and (2.7) yields

$$B_{if} = B_{fi} \qquad \text{[assuming no degeneracy]}$$

and

$$A_{fi} = \frac{8\pi h \nu_{if}^3}{c^3} B_{fi} \tag{2.8}$$

If there is degeneracy, then the equation relating the coefficients of stimulated emission and absorption is

$$g_i B_{if} = g_f B_{fi} \tag{2.9}$$

where

$$g_\alpha = (2J_\alpha + 1)$$

Therefore, if we could calculate A_{fi} in terms of observable quantities, we could determine B_{fi} and B_{if}. To do this, we examine the dipole moment of a molecule.

Letting $\vec{\mu}(t)$ denote the dipole moment

ψ_i - the wavefunction of the initial state

and ψ_f - the wavefunction of the final state,

then we define $\vec{\mu}_{if}$ (called the matrix element of the dipole moment between initial and final states) such that

$$\vec{\mu}_{if} = \int \psi_i^\dagger \vec{\mu}(t) \psi_f \, d^3x$$

The dipole moment is also equal to $e\vec{r}$ where e is the electric charge and $\vec{r}$ is the separation between two opposite charges.

$$\vec{\mu}_{if} = \int \psi_i^\dagger e\vec{r} \psi_f \, d^3x$$

Writing the wavefunction as a product of two functions, one of time and one of position

$$\psi = \phi(r)\, e^{i\omega t}.$$

Then $$\vec{\mu}_{if} = e \int \phi_i^{\dagger}(r)\, e^{-i\omega_i t}\, \vec{r}\, \phi_f(r)\, e^{i\omega_f t}\, d^3x$$

$$= e \int \phi_i^{\dagger}(r)\, \vec{r}\, \phi_f(r)\, e^{-2\pi i \frac{[E_i - E_f]t}{h}}\, d^3x.$$

Defining $\vec{r}_{if}$ as $\int \phi_i^{\dagger}(r)\, \vec{r}\, \phi_f\, d^3x$ and ν_{if} as $\frac{E_i - E_f}{h}$ in accordance with the Bohr transition rule, then

$$\vec{\mu}_{if} = e\, \vec{r}_{if}\, e^{-2\pi i\, \nu_{if}\, t}. \tag{2.10}$$

The power radiated from an atom is given by [22]

$$\underline{P} = \frac{2}{3c^3} \left| \overline{\ddot{\mu}} \right|^2.$$

Using (2.10) $$\underline{P} = e^2 |r|^2 16\pi^4 \nu_{if}^4.$$

Also, for an oscillating dipole [22]

$$|r|^2 = 2|\vec{r}_{if}|^2$$

so that

$$\underline{P} = \frac{4}{3c^3} (16\pi^4 \nu_{if}^4)\, e^2 |\vec{r}_{if}|^2. \tag{2.11}$$

From the Einstein transition probability, the radiated power is also given by

$$\underline{P} = h\, \nu_{fi}\, A_{fi}. \tag{2.12}$$

Therefore

$$A_{fi} = \frac{64\pi^4}{3\,hc^3}\ \nu_{if}^3\ e^2\ |\vec{r}_{if}|^2 . \qquad (2.13)$$

(2.13) and (2.8) together give us the desired relation

$$B_{if} = \frac{g_f}{g_i}\ \frac{8\pi^3}{3h^2}\ |\mu_{if}|^2 . \qquad (2.14)$$

We now digress for a moment to examine Clebsch-Gordon coefficients and the Wigner-Eckart Theorem as they will allow us to rewrite $|\mu_{if}|^2$ in terms of a rotationally averaged observable $|p^A{}_{if}|^2$.

Following the notation of Böhm [23], let the eigenvalues of J^2 for two angular momentum states $|j_1m_1>$ and $|j_2m_2>$ be $j_1(j_1+1)$ and $j_2(j_2+1)$ respectively.

i.e.
$$J^2|j_1m_1> = j_1(j_1+1)|j_1m_1>$$
$$J^2|j_2m_2> = j_2(j_2+1)|j_2m_2>$$
$$J_3|j_1m_1> = m_1|j_1m_1>$$
and
$$J_3|j_2m_2> = m_2|j_2m_2>$$

We define the uncoupled direct product of these two vectors as $|j_1m_1>\otimes|j_2m_2> = |j_1m_1j_2m_2>$ and the coupled direct product as $|jm>$. These two vectors are related by the general transformation

$$|jm> = \sum_{m_1,m_2} |j_1m_1j_2m_2><j_1m_1j_2m_2|jm>$$

The quantities $<j_1m_1j_2m_2|jm>$ are called "Clebsch-Gordon coefficients". Two important properties of Clebsch-Gordon coefficients will be stated

here but are derived in any elementary book an angular momentum [24], [25].

$$(1)\quad \langle j_1 m_1 j_2 m_2 | jm\rangle = 0 \quad \text{unless } m = m_1 + m_2 \qquad (2.15)$$
$$\text{and} \quad |j_1 + j_2| \geq j \geq |j_1 - j_2|$$

(2) the orthogonality relations between the coefficients are

$$\sum_{m_1 m_2} \langle j_1 m_1 j_2 m_2 | jm\rangle \langle j_1 m_1 j_2 m_2 | j'm'\rangle = \delta_{jj'}\, \delta_{mm'} \qquad (2.16)$$

and $$\sum_{jm} \langle j_1 m_1 j_2 m_2 | jm\rangle \langle j_1 m_1' j_2 m_2' | jm\rangle = \delta_{m_1 m_1'}\, \delta_{m_2 m_2'} \ .$$

The Wigner-Eckart Theorem states that the matrix element of an operator is equal to the product of a Clebsch-Gordon coefficient and a reduced matrix element [24].

$$\text{i.e.} \quad \langle j'm' | T^J_K | jm\rangle = \langle j'm'kJ | jm\rangle \langle j' || T^J || j\rangle$$

Here T^J is a tensor operator of rank J and k = (-J, -J+1 ... 0, ... J-1, J) denotes the spherical component of T^J.

Thus the matrix element of the dipole operator along the z axis is

$$\langle j'm' | \vec{\mu}^1_o | jm\rangle = \langle j'm'10 | jm| \rangle \langle j' || \mu || j\rangle \qquad (2.17)$$

We note immediately that $\langle j'm' | \mu^1_o | jm\rangle$ equals zero unless m' = m and j' = j±1. These are just the selection rules for dipole radiation. We also notice that the reduced matrix element $\langle j' || \mu || j\rangle$ is just the dipole strength defined previously as $|p^A_{jj'}|$.

According to Rose [20], equation (2.17) can be written in the following way

$$\langle j_i m_i | \mu_o | j_f m_f \rangle = \sqrt{\frac{(2J_i+1)}{(2J_f+1)}} \sum_{m_i} \langle j_i m_i 10 | j_f m_f \rangle \langle j_i 010 | j_f 0 \rangle \cdot |p_{if}^A|$$

$$= \mu_{if}$$

$$\therefore \quad |\mu_{if}|^2 = \sum_{m_i} \frac{(2J_i+1)}{(2J_f+1)} \langle j_i m_i 10 | j_f m_f \rangle \langle j_i m_i 10 | j_f m_f \rangle |\langle j_i 010 | j_f 0 \rangle|^2 \cdot |p_{if}^A|^2$$

From standard tables of Clebsch Gordon coefficients , we have

$$|\langle j_i 010 | j_f 0 \rangle|^2 = \left[\frac{J_i+1}{2J_i+1}\right]$$

Using the orthonormality relation (2.16), we find

$$\sum_{m_i} \langle j_i m_i 10 | j_f m_f \rangle \langle j_i m_i 10 | j_f m_f \rangle = \delta_{j_i j_f} = 1$$

$$\therefore \quad |\mu_{if}|^2 = \frac{(J_i+1)}{(2J_f+1)} |p_{if}^A|^2 \qquad (2.18)$$

Let us now return to the derivation of (2.1), equipped now with eqn (2.18).

If we assume that the contributions from all oscillators in a given volume of gas are simply additive, then the absorption is [22]

$$I_{ab} = N_i \, h\nu_{if} \, P \, B_{if}. \qquad (2.19)$$

Here I_{ab} is the intensity of absorbed radiation and the other quantities are as previously defined. For stimulated emission

$$I_{st} = N_i \, h\nu_{if} \, P \, B_{if} \left(\frac{g_i}{g_f} \frac{N_f}{N_i}\right) \tag{2.20}$$

The observed absorption is $I_{ab} - I_{st}$, or from (2.19) and (2.20)

$$I_{ab'} = N_i \, h\nu_{if} \, P \, B_{if} \left[1 - \frac{g_i}{g_f} \frac{N_f}{N_i} \right] \tag{2.21}$$

The integrated absorption per unit path length, per unit density (ρ) is defined as

$$\int \frac{\alpha(\omega)}{\omega} d\omega = \frac{I_{ab'}}{\rho c P \nu_{if}} = \frac{N_i h \, B_{if}}{\rho c} \left[1 - \frac{g_i}{g_f} \frac{N_f}{N_i} \right].$$

Using $N_f = g_f \, e^{-E_f/KT} \, [\rho N_o] \cdot 1/Q$

and $N_i = g_i \, e^{-E_i/KT} \, [\rho N_o] \cdot 1/Q$

where ρN_o = (Amagat density) x (Loschmidt's number)

= total number of molecules in the sample

and $Q = \sum_{\alpha} (2J_\alpha + 1) \, e^{-E_\alpha/KT}$ is the state sum,

$$\int \frac{\alpha(\omega)}{\omega} d\omega = [N_o] \, h \, \frac{B_{if}}{cQ} \left[g_i \, e^{-E_i/KT} - \frac{g_i}{g_f} g_f \, e^{-E_f/KT} \right]$$

$$= \frac{N_o h}{cQ} \, g_i \, B_{if} \left[e^{-E_i/KT} - e^{-E_f/KT} \right] .$$

From (2.14) and (2.18),

$$B_{if} = \frac{g_f}{g_i} \frac{8\pi^3}{3h^2} \frac{(J_i + 1)}{(2J_f+1)} |p^A_{if}|^2 .$$

$$\therefore \quad \int \frac{\alpha(\omega)}{\omega} \, d\omega = \frac{8\pi^3 N_o}{3hcQ} (J_i+1) \left[e^{-E_i/KT} - e^{-E_f/KT}\right] |p^A_{if}|^2$$

as required.

To put this equation into a useful form for analysing our data, we look at the integrated absorption coefficient in more detail. The absorption coefficient per unit path length per unit density, α, is defined by

$$I = I_o \, e^{-\alpha \ell \rho}$$

where I is the measured intensity through the sample gas

I_o is the measured intensity with no sample

ℓ is the pathlength

and ρ is the density.

$$\therefore \quad \alpha = 1/\ell\rho \; \ell n \, [I_o/I]$$

$$= 1/\ell\rho \; \ell n \, (10) \log_{10} [I_o/I]$$

$$= (2.303/\ell\rho) \log_{10} I_o/I$$

Using the definition of $\log_{10} I_o/I$ = Absorbance "X", and assuming the frequency is constant across an absorption line, we get the more useful analysing equation

$$\int X(\omega) d\omega = \left(\frac{\ell\rho}{2.303}\right) \left(\frac{8\pi^3 \omega N_o}{3hcQ}\right) (J_i+1) \left[e^{-E_i/KT} - e^{-E_f/KT}\right] |p^A_{if}|^2 . \qquad (2.22)$$

CHAPTER 3

INTRACOLLISIONAL INTERFERENCE

Collision induced spectra result from transient dipole moments that are created during the "collision" of a pair of interacting molecules. If one or both of these molecules has a permanent dipole moment, then interference between the two types of moments may result. This effect has been studied in detail by Tipping, Poll and their collaborators [7], [26] and [27] who denote this phenomenon "intracollisional interference".

At relatively low pressures, (as is the case in our experiments) we assume that the effect is proportional to the number of colliding pairs. Therefore it is sufficient to examine in detail the absorption due to one interacting pair and multiply the end result by the number of pairs. Using this model we define the matrix element of the dipole moment between initial and final states as

$$\langle i|\mu|f\rangle \equiv \mu_{if} = (\mu_{if}^{A})_1 + (\mu_{if}^{A})_2 + (\mu_{if}^{I}). \tag{3.1}$$

Here $(\mu_{if}^{A})_\alpha$ is the allowed dipole moment matrix element of particle α and (μ_{if}^{I}) is the induced dipole moment matrix element. Equation (2.1) indicates

$$\int \frac{\alpha(\omega)}{\omega}\, d\omega = K_{if}\, |\langle i|\mu|f\rangle|^2 \tag{3.2}$$

where

$$K_{if} = \frac{8\pi^3}{3hc}\, \frac{N_o}{Q}\, (2J_f + 1)\, [e^{-E_i/KT} - e^{-E_f/KT}] \tag{3.3}$$

and we have used (2.18) for $|p_{if}^{A}|^2$.

$$\therefore \int \frac{\alpha(\omega)}{\omega} d\omega = K_{if} [4(\mu_{if}^{A})^2 + (\mu_{if}^{I})^2 + 4(\mu_{if}^{A})(\mu_{if}^{I})], \qquad (3.4)$$

The $(\mu_{if}^{A})^2$ term yields sharp absorption lines while the $(\mu_{if}^{I})^2$ term gives the usual collision-induced broadband feature [7]. The $(\mu_{if}^{A})(\mu_{if}^{I})$ component gives rise to the intracollisional interference effect. Like the allowed spectrum, it results in sharp absorption lines that, depending on the relative signs of the two matrix elements, will either enhance or reduce the integrated intensity [7].

Concentrating only on the interference term, we write

$$\int_{\text{int}} \frac{\alpha(\omega)}{\omega} d\omega = 4 K_{if} (\mu_{if}^{A})(\mu_{if}^{I}).$$

According to Tipping et al., this can also be expressed as

$$\int_{\text{int}} \frac{\alpha(\omega)}{\omega} d\omega = [4 N_o] \frac{4\pi^2}{3hc} \sum_{if} P_i (\mu_{if}^{A})(\mu_{if}^{I}) \cdot [1 - e^{(+E_i - E_f)/KT}] \qquad (3.5)$$

where ρN_o is the total number of pairs in a volume V and $P_i = \frac{e^{-E_i/KT}}{Q}$.

Let us now examine closely the induced dipole moment matrix element (μ_{if}^{I}). If we treat the nuclear motion of the pair of interacting molecules adiabatically, then we can write the wavefunctions

$$\psi_i = \psi_{e\ell}^{o} (\vec{x}_1, \vec{x}_2; \vec{r}_1, \vec{r}_2, R) \phi_i(\vec{r}_1 \vec{r}_2, R).$$

Here $(\vec{x}_1, \vec{x}_2)$ are electronic coordinates

$(\vec{r}_1, \vec{r}_2)$ are nuclear coordinates in the center

of mass frame for a given molecule,

$\vec{R}$ is the vector joining the centers of mass of the interacting pair,

and $\psi_{e\ell}^{\circ}$ is the electronic wavefunction that satisfies

$$H_{e\ell}^{\circ}\, \psi_{e\ell}^{\circ} = U(\vec{r}_1, \vec{r}_2, R)\, \psi_{e\ell}^{\circ} .$$

$U(\vec{r}_1, \vec{r}_2, R)$ is then the usual Coulomb potential for the charge configuration.

The nuclear wavefunctions ϕ_i must satisfy the auxillary equation

$$(T + U)\, \phi_i = E_i \phi_i$$

where T is the kinetic energy operator of the nuclei and E_i is the eigenvalue of ϕ_i.

Tipping et al. rewrite the Coulomb potential as

$$U(\vec{r}_1, \vec{r}_2, \vec{R}) = V_1(\vec{r}_1) + V_2(\vec{r}_2) + V(\vec{r}_1, \vec{r}_2, R)$$

where $V_1(\vec{r}_1)$ and $V_2(\vec{r}_2)$ are the isolated molecule Born-Oppenheimer potentials and $V(\vec{r}_1, \vec{r}_2, R)$ is the intermolecular potential. Using this model, they write the spherical component of the induced dipole moment (μ_ν) for a fixed nuclear configuration

$$\mu_\nu^{I}(\vec{r}_1, \vec{r}_2, R) = \langle \psi_{e\ell}^{\circ} | \mu_\nu | \psi_{e\ell}^{\circ} \rangle .$$

The induced absorption is determined by the matrix elements $\langle \psi_{e\ell}^{\circ}\, \phi_i | \mu_\nu | \psi_{e\ell}^{\circ}\, \phi_f \rangle$, which reduce to $\langle \phi_i | \mu_\nu^{I} | \phi_f \rangle$.

This last expression is the same as (μ^I_{if}) if we neglect insignificant Born-Oppenheimer effects.

Next they expand μ^I_ν in terms of spherical harmonics as follows

$$\mu^I_\nu = \frac{(4\pi)^{3/2}}{\sqrt{3}} \sum_{\lambda_1\lambda_2\Lambda\lambda} A_\Lambda(\lambda_1\lambda_2\lambda;\, r_1 r_2 R) \sum_{\alpha,\beta} C(\lambda_1\lambda_2\Lambda;\, \nu-\alpha-\beta,\beta)\, C(\Lambda\lambda 1;\, \nu-\alpha,\alpha)\, Y_{\lambda_1}(\nu-\alpha-\beta) Y_{\lambda_2\beta}\, Y_{\lambda\alpha}\,. \tag{3.6}$$

Here the C's are Clebsch-Gordon coefficients and the A's are unknown functions. (λ_1, λ_2 and λ) are angular momentum eigenvalues (like j_1, j_2 and j), (α, β, ν) are the projections of (λ_1, λ_2 and λ) (like m_1 m_2 and m) and $\Lambda = (-\lambda, -\lambda + 1 \ldots 0 \ldots \lambda)$ are spherical components of the functions A.

Tipping and Poll make the following assumptions to construct the ϕ_i's

(1) replace the internuclear distances in $V(\vec{r}_1, \vec{r}_2, R)$ by their equilibrium values $\vec{r}_{1e}$, $\vec{r}_{2e}$.

i.e. $V(\vec{r}_1,\vec{r}_2,R) = V(\vec{r}_{1e}\vec{r}_{2e}R)$.

(2) in the resulting potential V, consider only the isotropic part. i.e. Use only $V(\vec{r}_{1e}\ \vec{r}_{2e}, R) = V(R)$.

As a result of these approximations, the nuclear and translational motions separate.

$$\therefore \quad \phi_i = Y_{J_1 m_1}\, Y_{J_2 m_2}\, \chi_{v_1 J_1}(r_1)\, \chi_{v_2 J_2}(r_2)\, F_{nL}(R)\, Y_{LM}\,. \tag{3.7}$$

The functions χ are the unperturbed Born-Oppenheimer vibrational wave functions and $F_{nL}(R)$ describes the relative motions of the centers of mass. Combining (3.6) and (3.7) yields the quantity (μ^{I}_{if}). Thus the contribution of the interference term to the integrated intensity per unit length per unit density can be written, alternatively to (3.5),

$$\int_{\text{int.}} \frac{\alpha(\omega)}{\omega}\, d\omega = 4\, \frac{(N_o)\, 4\pi^2}{3hcQ} \left[e^{-E_i/KT} - e^{-E_f/KT}\right] \sum_{if} (\mu^{I}_{\nu if})(\mu^{A}_{\nu if}). \tag{3.8}$$

Performing the sum of m_1, m_1', m_2 and m_2' over the components of ν and setting $J_2 = J_2'$, $m_2' = m$, yields

$$\Sigma(\mu^{I}_{\nu if})(\mu^{A}_{\nu if}) = (J + 1)\, |p^{A}_{v_1 J_1 v_1' J_1'}|\, (2L + 1)(2J_2 + 1)$$
$$\langle F_{nL} | p^{I}_{v_1 J_1 v_1' J_1'} | F_{nL} \rangle \tag{3.9}$$

where the induced dipole strength is given by

$$p^{A}_{v_1 J_1 v_1' J_1'} = \langle v_1' J_1' | A_1(100;\, r_1 r_{2e} R) | v_1 J_1 \rangle \tag{3.9a}$$

and $A_1(100;\, r_1 r_{2e} R)$ has been defined by the expansion (3.6).

(3.7), (3.8) and (3.9) together given a new expression for the integrated intensity per unit length per unit density

$$\int_{\text{int}} \frac{\alpha(\omega)}{\omega}\, d\omega = \frac{16\pi^2 (N_o)}{3hcQ} \left[e^{-E_i/KT} - e^{-E_f/KT}\right] (J + 1)\, p^{A}_{v_1 J_1 v_1' J_1'}$$
$$\cdot\, 4\pi \int_0^{\infty} g(R)\, p^{I}_{v_1 J_1 v_1' J_1'}\, R^2 dR$$

where $g(R) = V \sum_{nL} \frac{(2L+1)}{4} F^2_{nL}(R) P_{nL}$ and P_{nL} is a translational Boltzmann factor with normalization $\sum_{nL} (2L+1) P_{nL} = 1$.

Considering now the total number of colliding pairs (equals $\frac{(\rho N_o)}{2}$), they write the total integrated absorption due to intracollisional interference per unit length per unit density

$$\int \frac{\alpha(\omega)}{\omega} d\omega = \frac{8\pi^2}{3hcQ} \rho(N_o)^2 [e^{-E_i/KT} - e^{-E_f/KT}] (J + 1)$$

int.total

$$P^A_{v_1 J_1 v'_1 J'_1} \cdot 4\pi \int_o^\infty g(R) P^I_{v_1 J_1 v'_1 J'_1} R^2 dR. \qquad (3.10)$$

Now let us examine $(\mu_{if}{}^I)$ in the case of pure HD. In an H_2 molecule, the midpoint coincides with the center of mass, while in an HD molecule they do not. Figure 3 shows a pair of HD molecules interacting.

Figure 3. THE HD-HD INTERACTION

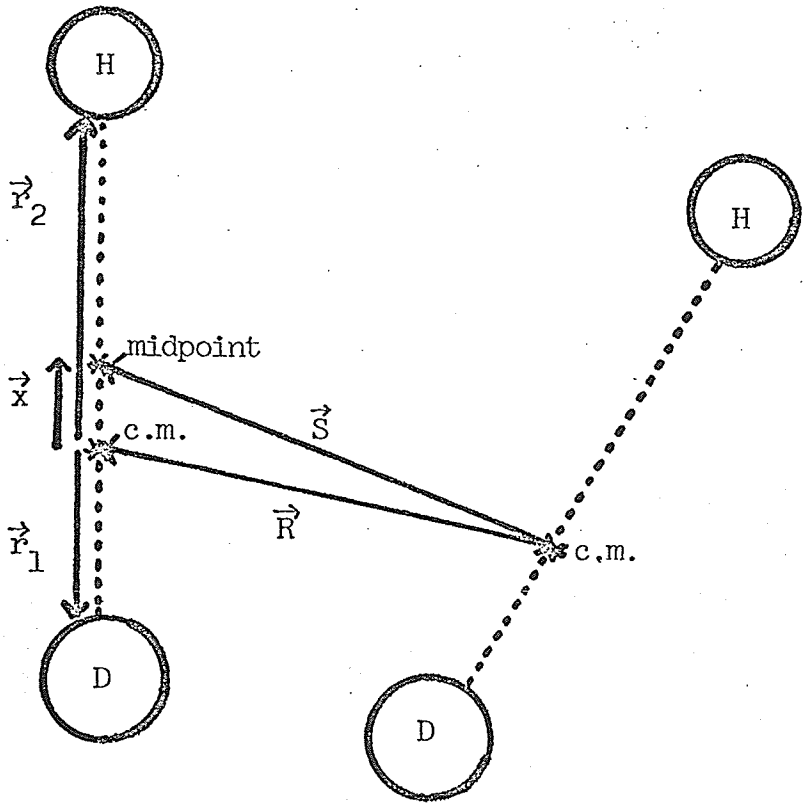

A straightforward calculation yields

$$\vec{x} = 1/6(\vec{r}_2 - \vec{r}_1)$$

$$\therefore \quad \vec{S} \approx \vec{R} + \vec{x}$$

To first approximation, then, we write

$$\mu^I_{HD} = [1 + \vec{x} \cdot \nabla_R] \mu^I_{H_2} \tag{3.11}$$

where we have considered μ^I_{HD} to be a small perturbation from that of H_2. It has been shown by Tipping et al. [7] that the $A_2(201:r_1r_2R)$ component of pure H_2 will give rise to an $A_1(100:r_1r_2R)$ component in HD. They assumed a model of the form

$$A_2(201;r_1r_2R) = A_2(r_1,r_2)\, e^{-(R-\sigma)/\delta}$$

where $A_2(r_1,r_2)$ is the strength of the dipole at the Lennard-Jones diameter σ, and δ specifies the range of interaction. Thus, for the purpose of differentiation, they chose

$$\mu^I_{H_2} = A_2\, e^{-(R-\sigma)/\delta}\, \vec{R}/R .$$

Then [28],

$$\begin{aligned}
\mu^I_{HD} &= [1 + (\vec{x} \cdot \nabla_R)](A_2\, e^{-(R-\sigma)/\delta}\, \vec{R}/R) \\
&= A_2(-1/\delta)\, e^{-(R-\sigma)/\delta}\, \vec{x} \cdot \vec{R}/R \;\; \vec{R}/R \\
&+ A_2\, 1/R\, e^{-(R-\sigma)/\delta} \vec{x} - A_2\, e^{-(R-\sigma)/\delta} \vec{x} \cdot \vec{R}/R \;\; \vec{R}/R \\
&= A_2(-1/R - 1/\delta)\, e^{-(R-\sigma)/\delta} \vec{x} \cdot \vec{R}/R \;\; \vec{R}/R \\
&+ A_2\, 1/R\, e^{-(R-\sigma)/\delta} \vec{x} .
\end{aligned} \tag{3.12}$$

Notice however that $\vec{Z} = \vec{x} \cdot \vec{R}/R \ \vec{R}/R$ contains a component that is independent of $\vec{R}$. To see this, take

$$\vec{x} \cdot \vec{Z} = [\vec{x} \cdot \vec{R}/R]^2$$

$$= x^2 \cos^2 \gamma$$

where γ is the angle between the two vectors $\vec{x}$ and $\vec{R}$. But $P_2(\cos \gamma) = 1/2\ (3\cos^2\gamma - 1)$ so that $\cos^2\gamma = 1/3 + 2/3\ P_2(\cos \gamma)$. If we average over all orientations for the pair of interacting molecules (i.e. over a sphere), we're left with

$$\langle \cos^2\gamma \rangle_{\text{sphere}} = 1/3 \ .$$

$$\therefore \quad \langle \vec{x} \cdot \vec{Z} \rangle_{\text{sphere}} = 1/3\ x^2$$

or the isotropic component of $\vec{Z} = 1/3\ \vec{x}$. Using only this isotropic component in (3.12) yields

$$\mu^I_{HD} = [\mu^I_{H_2} + A_2/3(-1/R - 1/\delta)\ e^{-(R-\sigma)/\delta}\ \vec{x} + A_2\ 1/R\ e^{-(R-\sigma)/\delta}\ \vec{x}]$$

$$\text{or} \quad \mu^I_{H_2} = \mu^I_{H_2} + A_2/3\ [2/R - 1/\delta]\ e^{-(R-\sigma)/\delta}\ \vec{x} \qquad (3.13)$$

The first term is just the broadband induced background while the second term contributes to the intracollisional interference.

Tipping et al. have shown that the $A_2(201;\ r_1 r_{2e}\ R)$ component gives rise to an $A_1(100;\ r_1 r_{2e}\ R)$ component in HD [4]. Using (3.13), the form of $A_1(100;\ r_1 r_{2e}\ R)$ is

$$A_1(100:r_1 r_{2e}\ R) = A_2(r_1 r_2)\ 1/18(2/R - 1/\delta)\ e^{-(R-\sigma)/\delta}\ (\vec{r}_2 - \vec{r}_1). \qquad (3.14)$$

From (3.9a) and (3.14), the dipole strength in the ground vibrational state is

$$P^{I}_{0J_1 0J_1'} = \langle 0J_1' | A_1(100;\ r_1 r_{2e}\ R) | 0J_1 \rangle$$

$$= \langle 0J_1' || (\vec{r}_2 - \vec{r}_1) | A_2(r_1 r_{2e}) | 0J_1 \rangle\ 1/18\ (2/R - 1/\delta)\ e^{-(R-\sigma)/\delta}. \qquad (3.15)$$

Ab initio calculations of the ground vibrational dipole moment of HD [1], [3] indicate that the J-dependence is negligible. Also the quantity $A_2(r_1\ r_{2e})$ was defined as the dipole strength at $R = \sigma$ for pure H_2. Tipping Poll et al. found the following quantities for H_2

$$|A_2(r_1\ r_{2e})| = .65 \times 10^{-2}\ D \qquad (3.16a)$$

and

$$\delta/\sigma = .11\ . \qquad (3.16b)$$

To find the pressure dependence of the intracollisional interference, they expressed the integrated absorption per unit length per unit density in this form

$$\int \frac{\alpha(\omega)}{\omega}\, d\omega = \int \frac{\alpha^A(\omega)}{\omega}\, (1 + a\rho)\, d\omega \qquad (3.17)$$

where $\int \frac{\alpha^A(\omega)}{\omega}\, d\omega$ is the allowed integrated absorption

and $\int \frac{\alpha^A(\omega)}{\omega}\, (a\rho)\, d\omega$ is the integrated absorption due to the interference at a density ρ.

Combining (3.10) (3.15), and (3.17) gives

$$\int \frac{\alpha^{A}(\omega)}{\omega}(a\rho) = \frac{8\pi^2}{3hcQ}\rho(N_o)^2 (J+1)\left[e^{-E_i/KT} - e^{-E_f/KT}\right] P^{A}_{v_1J_1v_1'J_1'}$$

$$\cdot 4\pi \int_o^\infty g(R)\, R^2\, P^{I}_{v_1J_1v_1'J_1'}\, dR$$

Using (2.1) for $\int \frac{\alpha^{A}(\omega)}{\omega} d\omega$, they expressed the intracollisional interference parameter "a" as

$$a = \frac{8\, N_o}{P^{A}_{v_1J_1v_1'J_1'}} \int_o^\infty g(R)\, P^{I}_{v_1J_1v_1'J_1'}(R)\, R^2\, dR \qquad (3.18)$$

Tipping et al. assumed a Lennard-Jones potential with $\varepsilon = 37$ K and $\sigma = 2.928$ Å to calculate g(R). Using the theoretical value of Wolniewicz [1] of $|P^{A}_{0J0J'}| = 8.4 \times 10^{-4}$ D, they calculated $|a| = 5.4 \times 10^{-3}$ Amagat^{-1}.

CHAPTER 4

THE EXPERIMENT

The experiments were carried out at 1 cm^{-1} resolution on a modified Michelson interferometer manufactured by the Nicolet Instrument Corporation (see Fig. 4) [29].

A black-body source (S1) emits a broad band spectrum including a small flux of far infra-red radiation. The emitted radiation hits a beamsplitter (BS1) and forms two perpendicular beams. The first strikes mirror (M2) and returns to the beamsplitter. Here part of the beam passes through towards mirror (M5) and the other is reflected back to the source. The second beam strikes the moving mirror assembly and is reflected back along its incident path to the beamsplitter. Again some light is directed towards mirror (M5) and the remainder back to the source. The two beams travelling towards mirror (M5) interfere with each other.

After the "interference beam" is reflected by mirrors (M6) and (M7), it is focused onto the entrance window of the sample cell by mirror (M8). It passes through the gas cell, exciting the molecules and thereby further modulating the beam. The beam leaves the exit window of the gas cell and is focused by mirrors (M9) and (M10) into a detector (D1). The detector responds to the beam and sends a time-averaged modified interference pattern (known as an interferogram) to the computer.

Under appropriate commands from the operator, the computer then performs a fast-Fourier transform on the inerferogram to calculate

FIGURE 4 THE APPARATUS

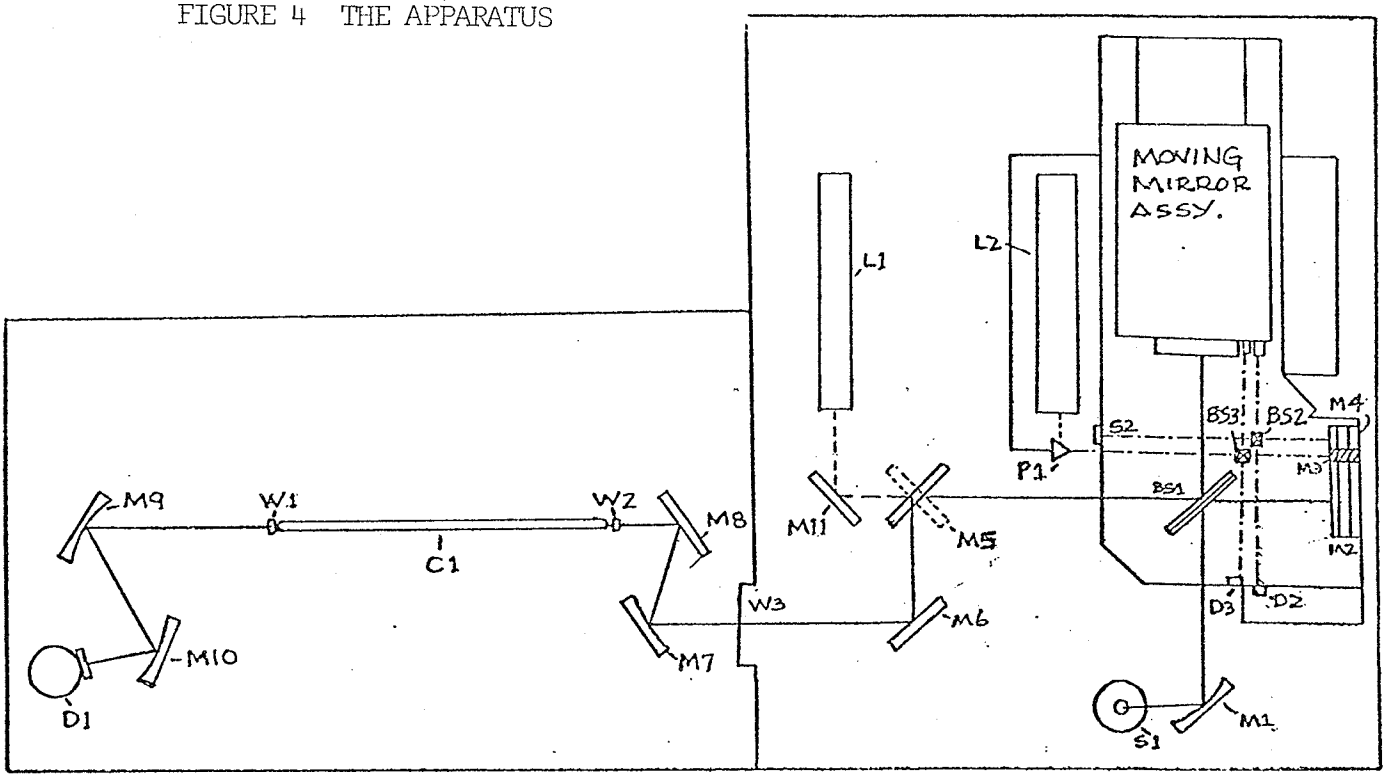

S1 - IR source

S2 - White light source

L1 - Allignment laser

L2 - Laser signal source

BS1 - IR beamsplitter

BS2 - White light beamsplitter

BS3 - Laser beamsplitter

D1 - IR detector

D2 - White light detector

D3 - Laser detection

C1 - Cell

W1 - Window (5.0 mm thick)

W2 - Window (5.0 mm thick)

W3 - Polyetheylene sheet (1.0 mm thick)

M1 - Spherical mirror 3.5" E.F.L.

M2 - Fixed flat mirror

M3 - Fixed flat mirror

M4 - Fixed flat mirror

M5 - 4-position flat mirror

M6 - Flat mirror

M7 - Spherical mirror 9.0" E.F.L.

M8 - Flat mirror

M9 - Spherical mirror 9.0" E.F.L.

M10 - Spherical mirror 3.5" E.F.L.

M11 - Flat mirror

the transmittance spectrum. By comparing two transmittance spectra—one with the sample gas in the cell and one without—the absorption spectrum of the sample gas can be determined.

The laser and white light systems that parallel the infrared interferometer act to coordinate the motion of the moving mirror assembly and the "channel advance" in the computer memory.

The laser beam passes through beamsplitter (BS3), strikes mirror (M3) and the moving mirror assembly. The two beams return to the beamsplitter (BS3) where part of each is directed towards the detector (D3). They interfere with each other in the same fashion as the IR beams do. Because the laser light is essentially monochromatic, the interference pattern is a sine wave. When the detector (D3) records a pre-determined number of zero-crossings (as set by the operator), a signal is sent to the computer advancing its memory to the next channel.

White light contains many frequencies so its interference pattern has one very large maxima. After passing through beamsplitter (BS2), hitting the appropriate mirrors (M4 and the moving mirror assembly) and passing through the beamsplitter again, the white light interference beam strikes detector (D2). This spike triggers the sampling mechanism i.e. it starts the data acquisition for each pass of the moving mirror. Thus the white light system controls the taking of data and the laser system controls the storage of that data.

To get an accurate low-noise spectrum, over a given frequency interval,all components in the system must optimized for transmittance. Several different sources, beamsplitters and detectors are available from the manufacturer of the interferometer and their characteristics are given in Figs. 5, 6 and 7.

As we were primarily interested in the 50 - 500 cm^{-1} frequency interval, we chose the globar as our source. It was connected to a regulated power supply with an output of 5 amps at 25 volts. The detector output signal was relatively insensitive to small changes in the supply settings.

The beamsplitter chosen was a 6.25 micron mylar film equally stressed across a metal ring. Although the literature provided to us by Nicolet indicated that the 12.5 micron beamsplitter would be better suited to the region under 200 cm^{-1} we didn't find this to be the case. As the 6.25 micron beamsplitter transmitted over a sufficient region to see the R(1) through R(3) lines of HD with some degree of confidence, we decided to use it exclusively.

The detector used was a TGS-(PE) as it operated over a wide frequency range with no need for specific operating conditions. (i.e. low temperatures)

The gas cellused was similar in design to that suggested by Horne and Birnbaum [30] (see Fig. 8). It was a 1.00 meter long stainless steel tube with an inner diameter of 1.3 cm and an outer diameter of 1.9 cm. End pieces of stainless steel (6.3 cm outer diameter) were welded onto the tube to act as supports to which windows

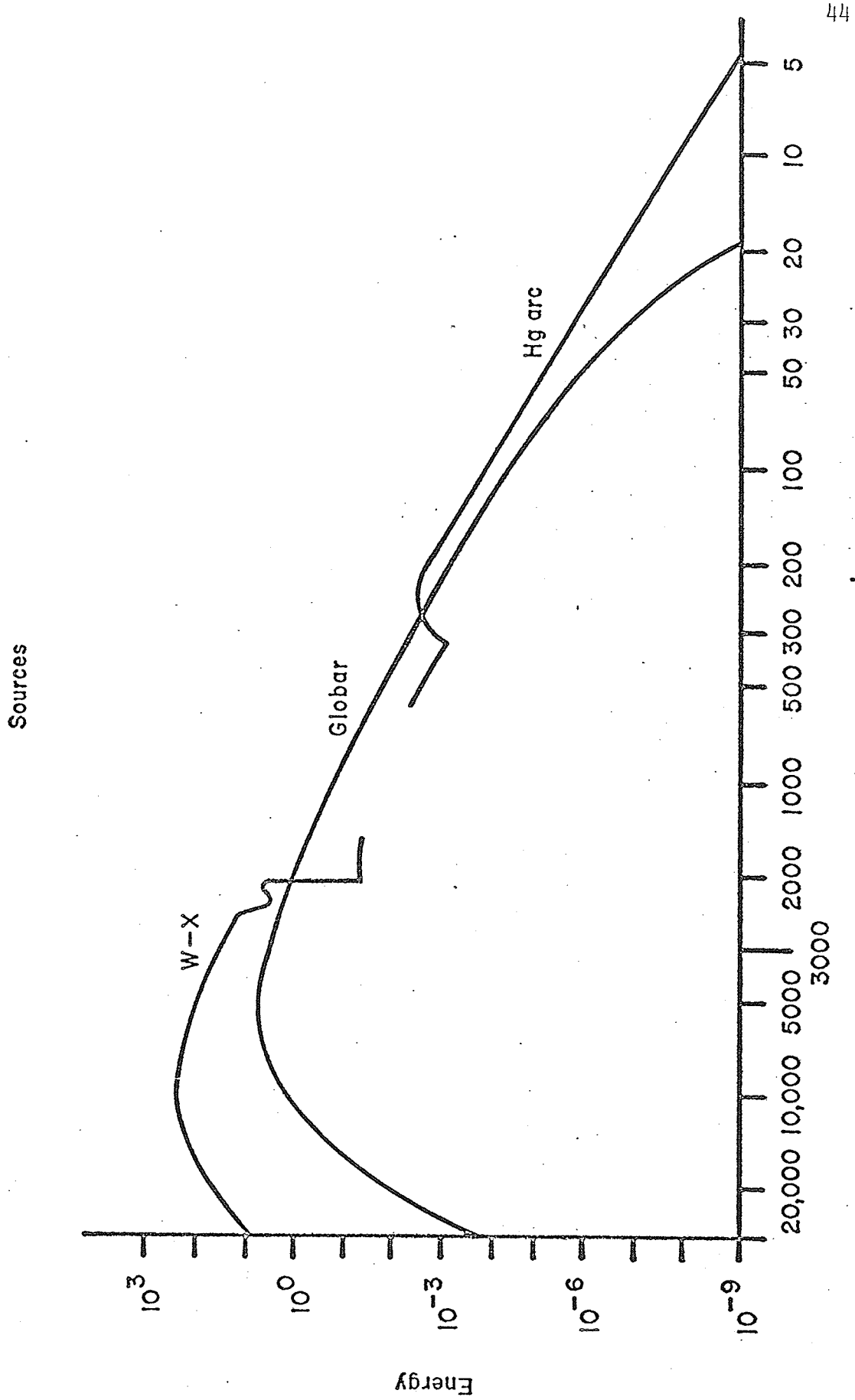
Sources
W-X
Globar
Hg arc
Energy
10^{3}
10^{0}
10^{-3}
10^{-6}
10^{-9}
20,000 10,000 5000 3000 2000 1000 500 300 200 100 50 30 20 10 5
Wavenumbers cm^{-1}

FIGURE 5

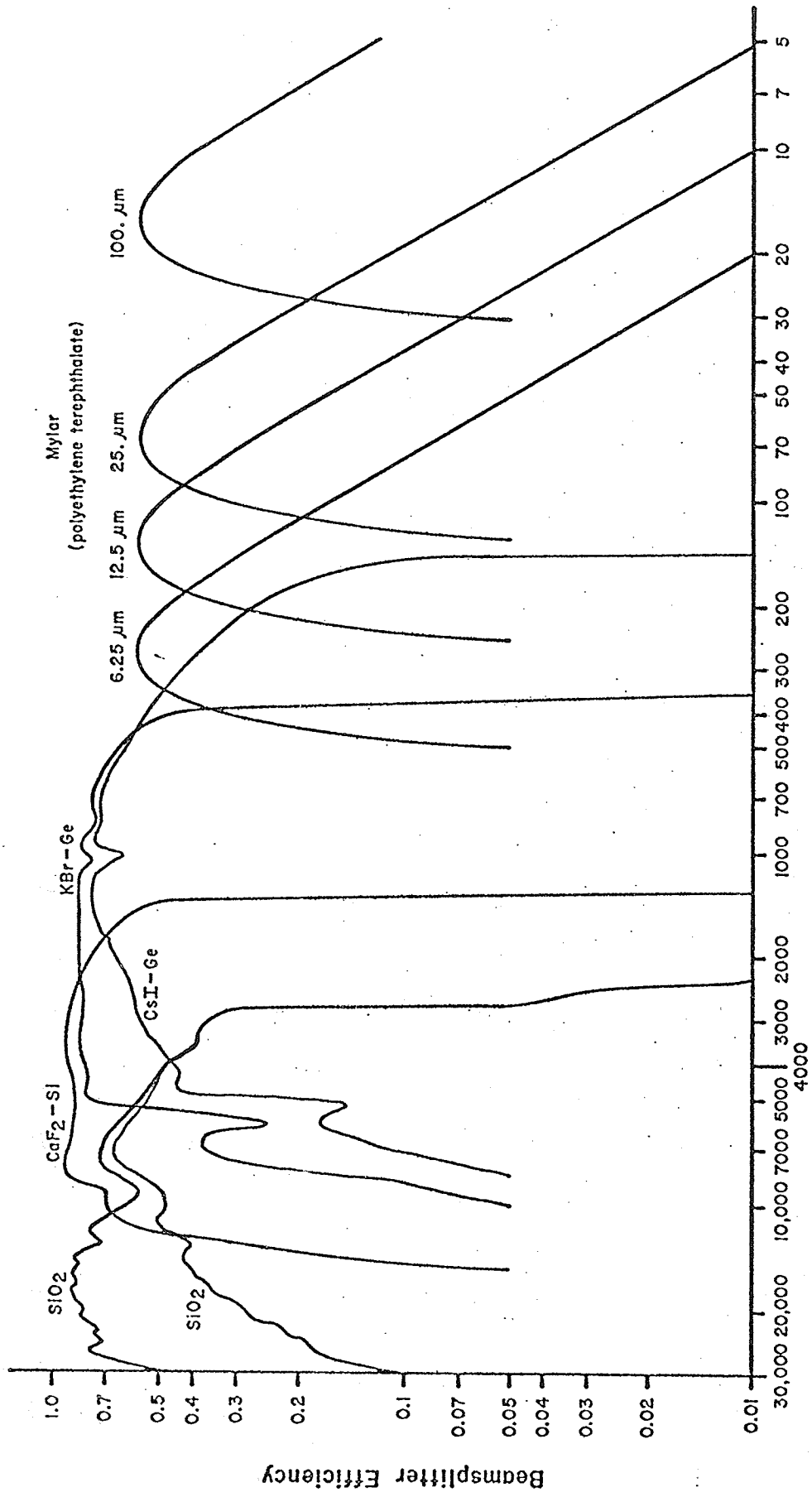
Beamsplitter Efficiencies
Beamsplitter Efficiency
Wavenumbers cm⁻¹
SiO2
CaF2 - SI
KBr - Ge
CsI - Ge
SiO2
Mylar
(polyethylene terephthalate)
6.25 µm
12.5 µm
25. µm
100. µm
1.0
0.7
0.5
0.4
0.3
0.2
0.1
0.07
0.05
0.04
0.03
0.02
0.01
30,000 20,000 10,000 7000 5000 4000 3000 2000 1000 700 500 400 300 200 100 70 50 40 30 20 10 7 5

FIGURE 6

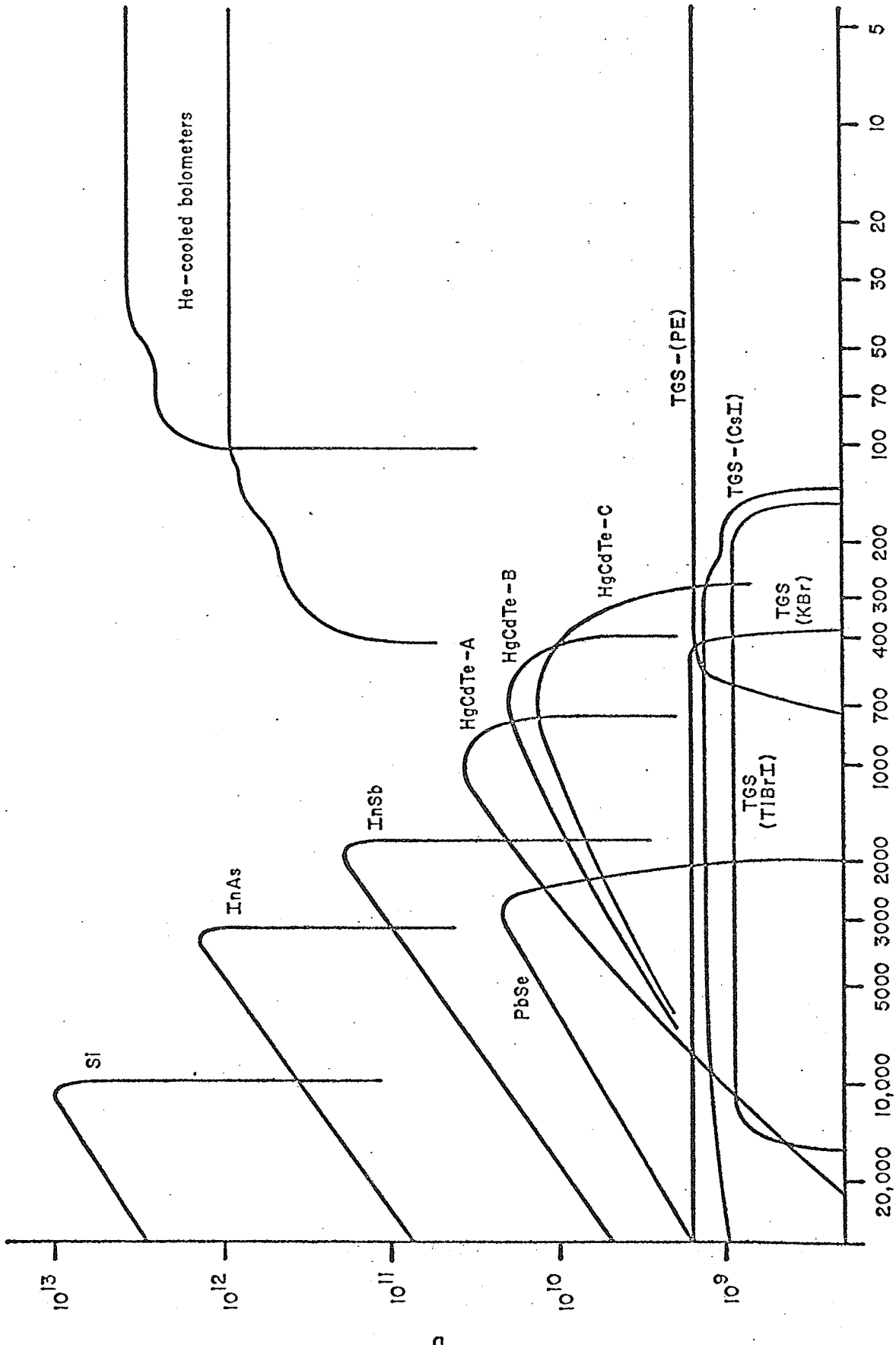
Sensitivity Ranges of Detectors
He-cooled bolometers
Si
InAs
InSb
PbSe
HgCdTe-A
HgCdTe-B
HgCdTe-C
TGS-(PE)
TGS-(CsI)
TGS (KBr)
TGS (TlBrI)
D*
Wavenumbers cm⁻¹
10¹³
10¹²
10¹¹
10¹⁰
10⁹
20,000
10,000
5000
3000
2000
1000
700
400
300
200
100
70
50
30
20
10
5

FIGURE 7

FIGURE 8 HIGH PRESSURE SAMPLE CELL

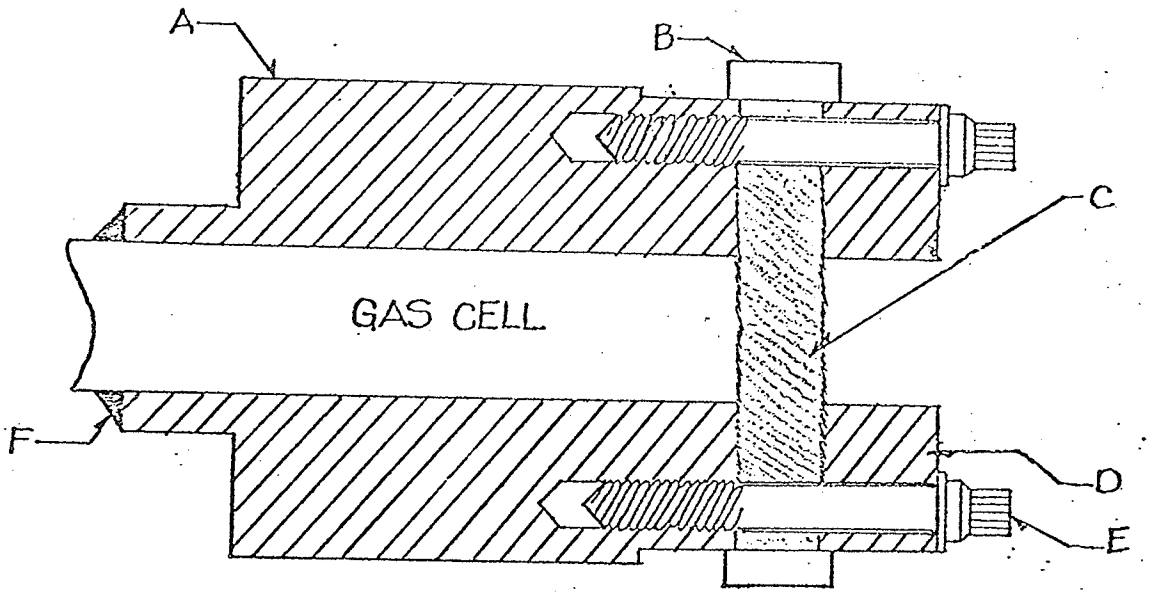

A - gas cell flange, stainless steel 6.3 cm diameter

B - external retainer ring for polyetheylene seal

C - high density polyethylene window 5.0 mm thick

D - light pipe flange

E - bolt, 6 equally spaced bolts are used

F - weld between cell and flange

could be attached.

A high density polyethylene disk (of variable thickness),(C) was compressed between the two flanges (A and D). Six bolts (E) tightly clamped the two flanges together. Five concentric grooves (about 0.5 mm in depth) cut into each flange allowed the stressed polyethylene disks to flow, thereby creating their own O-rings. A retaining ring (B) constrained the flow to the grooves.

The inside of the cell was polished with steel wool to create its own light pipe. Several short pieces of gold-plated glass tubing (1.0 cm in diameter) were butted together inside the cell to form an auxilliary light pipe. The detector signal was enhanced by only a few percent by this pipe and its net effect was deemed negligible. Thus in the experiments carried out, only the polished cell was used as a waveguide.

The transmittance of polyethylene in the 50 - 500 cm^{-1} region is almost uniform but drops significantly with thickness. With both windows(5.0 mm thick) in place, the signal at the detector was only about 15% of that with no windows on the cell. Thinner windows could have been used but in the interests of safety when working with high pressure gases, we chose not to.

Pressure tests with nitrogen indicated that the cell was leak free at 1500 p.s.i. for a period of 24 hours and for several days at lower pressures. It was also tested under vacuum and held for several days.

Welded near one end of the cell was a male high pressure connection from Aminco. This was attached to a four opening female connector, to which an inlet valve, an outlet valve and a pressure gauge were connected. The inlet valve went directly to the sample bottle while the outlet valve was attached to a vent line. The vent line ran outdoors to eliminate the escape of flammable gas into the room. The pressure gauges used were: 0-3000 p.s.i. made by Maxisafe and 0-85 p.s.i. made by Matheson. Both gauges were calibrated by personnel of the Dept. of Mechanical Engineering at the University of Manitoba.

As a precaution against HD leaking out of the cell and back into the main interferometer, a 1.0 mm thick sheet of polyethylene was fastened over the opening in the interferometer housing (between mirros M6 and M7). The signal intensity was reduced by 10% with the sheet in place.

As the infra-red spectrum of water has many features in our region of interest, special precautions had to be taken to eliminate water from the system. Aluminum covers were constructed to house the pre-cell optics (mirrors M8 and M7) and the detection optics (mirrors M9, M10 and the detector D1). All connections were sealed with tape and a sealing compound to make them as airtight as possible. Liquid nitrogen was boiled into both housings and the main interferometer to purge the system of water vapor. After 24 hours of continuous purging, the water level reached its minimum level and the experiment could be run.. Continued purging was required though,

to maintain that minimum level.

The HD sample gas was obtained from Merck, Sharpe and Dhome Canada Limited in Montreal. Although it was reputed to be research grade, it was found to contain enough water to completely mask our results. To remove the water, we submersed the entire 50 ℓ cylinder in a liquid nitrogen cold trap. After the cylinder's temperature was reduced sufficiently and the water in the sample had frozen, the dry sample could be released slowly into the system.

To provide a background absorption spectrum, the cell was evacuated through the outlet valve. A roughing pump capable to creating a 10 micron vacuum was used for this purpose and after several minutes of pumping, the minimum pressure was reached. Closing off the outlet valve maintained the vacuum.

Preliminary experiments were carried out using N_2 and H_2 to test the equipment. Neither of these gases exhibit allowed rotational features, but at sufficiently high pressures (> 20 atmospheres) collision-induced rotational spectra are observed. These broad band spectra lie in the 100 - 700 cm^{-1} region. Reproduction of the results of Kiss et al. [31] and Harries [32] demonstrated the systems reliability.

The HD experiments were run continuously for several days on two separate occasions. The system was purged for two days before and continuously during the runs. For run "B", the cell was evacuated for approximately one hour prior to the taking of data. A background run was completed using 4000 scans to find the transmittance spectrum of

the system.

Immediately after gathering the background data, a small amount (<5 atmospheres) of HD was admitted into the high pressure cell through a liquid nitrogen trap. A short run ($\simeq$ 500 scans) confirmed that the trap had frozen the water out of the HD. At this point the cell was charged to maximum bottle pressure, again through the liquid nitrogen.

The sample data was gathered over the next several days. After 4000 scans ($\simeq$ 6 hours of acquisition time) a small amount of HD was vented, thereby reducing the pressure in the cell. This process was repeated eleven times between the pressures of 32 and 4 atmospheres. Finally the cell was evacuated for approximately 1 hour before doing a second background run. Comparison of the first and second background runs indicated that the system had remained stable throughout the 4 days of use.

For run "A", carried out four months later, the same general procedure was followed. The pressures used on this occasion ranged between 5 and 65 atmospheres, involving 10 separate runs. Again the entire set of experiments were carried out over a four-day period.

In each case the experimental parameters were set as follows:

NSS = 4000

VEL = 15

GAN = 16

NDP = 2000

NTP = 8000

NPD = 60

NPT = 256

SSP = 16

FSZ = 22,000

LPS = 3

HPS = 0

SGH = 1

SGL = 1

PHZ = PH

AFN = HG

BDL = 30

COR = NO

Resolution = 2 x Bandwidth/NDP = 1 cm^{-1}

NSS - determines the number of scans that the computer averages to get the final interferogram. Because the signal-to-noise ratio (S/N) is proportional to the square root of the number of scans, we chose NSS = 4000 as a compromise between statistical noise and experiment duration.

VEL - sets the moving mirror velocity during the scan. In general, the slower the mirror velocity, the higher the resolution. Again we chose VEL = 15 (actual velocity = 0.160 cm/s [from Nicolet manual [29]]) as a trade-off between resolution and experiment duration.

GAN - refers to the instruments real gain before filtering. We chose GAN = 16 so as to observe the interferogram on individual scans.

NDP - determines the number of data points in the interferogram to be digitized. We chose NDP = 2000 to ensure accurate transforms without wasting computer time.

NTP - sets the number of Fourier transform points. All points not included by NDP are set to zero (up to the value of NTP) so as to better approximate an infinite interferogram. We set NTP = 8000.

NPD - specifies the number of points around the zero path difference to be used in constructing a smooth phase array. This parameter was set by Nicolet for optimum results in the far-IR [29].

NPT - specifies the number of points used in transforming the interferogram for phase correction. This too was set at its optimum value by the manufacturer.

SSP - determines the number of laser signal zero-crossings between each sampling point. At SSP = 16, the effective bandwidth is 1000 cm^{-1}.

FSZ - is the file size. It was set at 22000 to ensure ample memory space for all calculations.

LPS and HPS respectively determine the low and high pass filter roll-off frequencies to optimize S/N. These were set according to the manufacturer's literature.

SGL - determines the relative gain of the first 4352 data points while SGH determines the relative gain of the remaining points. Together they enhance the dynamic range of the interferogram by preventing ADC overflow. Both were set at 1 on recommendation by the manufacturer.

BDL - is the delay time between beam disruption and start of data acquisition. BDL = 30 refers to a start up delay time of 30 seconds after mirror adjustments etc.

COR = NO was used because the interferogram was visible on each scan. Only when the individual interferograms are very noisy or indistinct is it suggested that the computer compare the last interferogram to the time averaged results of the previous interferograms. In this way "poor" data could be disregarded.

APN - determines the apodization function to be applied to the data before transformation. To achieve a reasonable compromise between lineshape and resolution, we chose the Happ-Genzel function:

$$0.54 + 0.46 \cos \pi/2 \, [h_i - z/NDP - z]$$

where h_i is the displacement of the i'th data point from the start of scan, z is the zero path difference peak and NDP is the total number of data points.

PHZ - determines the phase correction algorithm to be used. Set at PH, the computer calculates the correction based on the real part of the transformation while the imaginary component is discarded.

Figure 9 shows a typical interferogram, time averaged over 4000 scans. Figure 10 shows the transmittance spectrum of the equipment. The sharp "valleys" in the spectrum correspond to water lines. These,

FIGURE 9

This is a typical interferogram averaged over 4000 scans, taken with low pressure HD in the sample cell.

FIGURE 9. THE INTERFEROGRAM

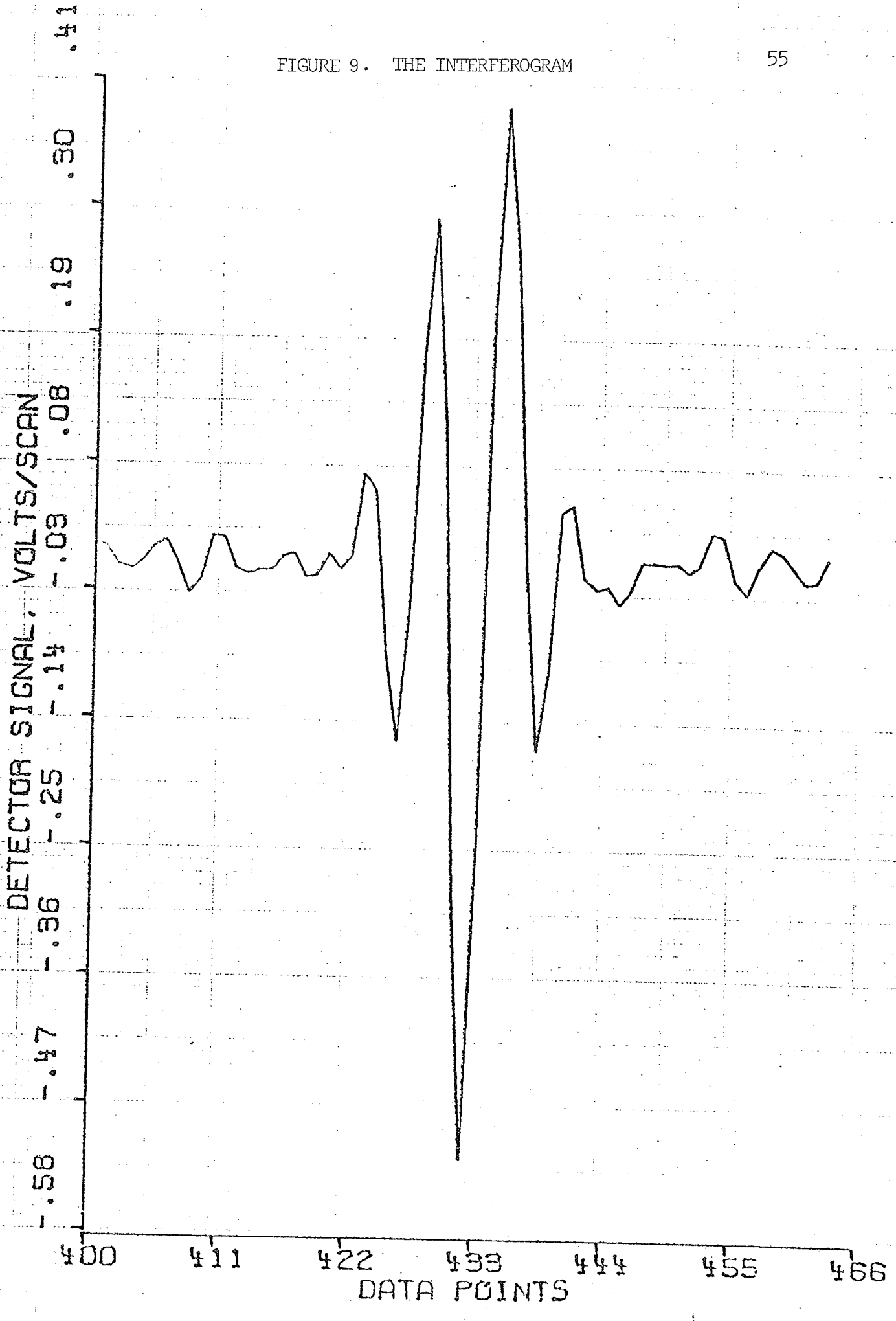

FIGURE 10

The transmission curve of the system with no HD in the cell is given. The sharp absorption lines are due to water. The ordinant is in arbitrary units.

FIGURE 10 THE BACKGROUND TRANSMITTANCE SPECTRUM

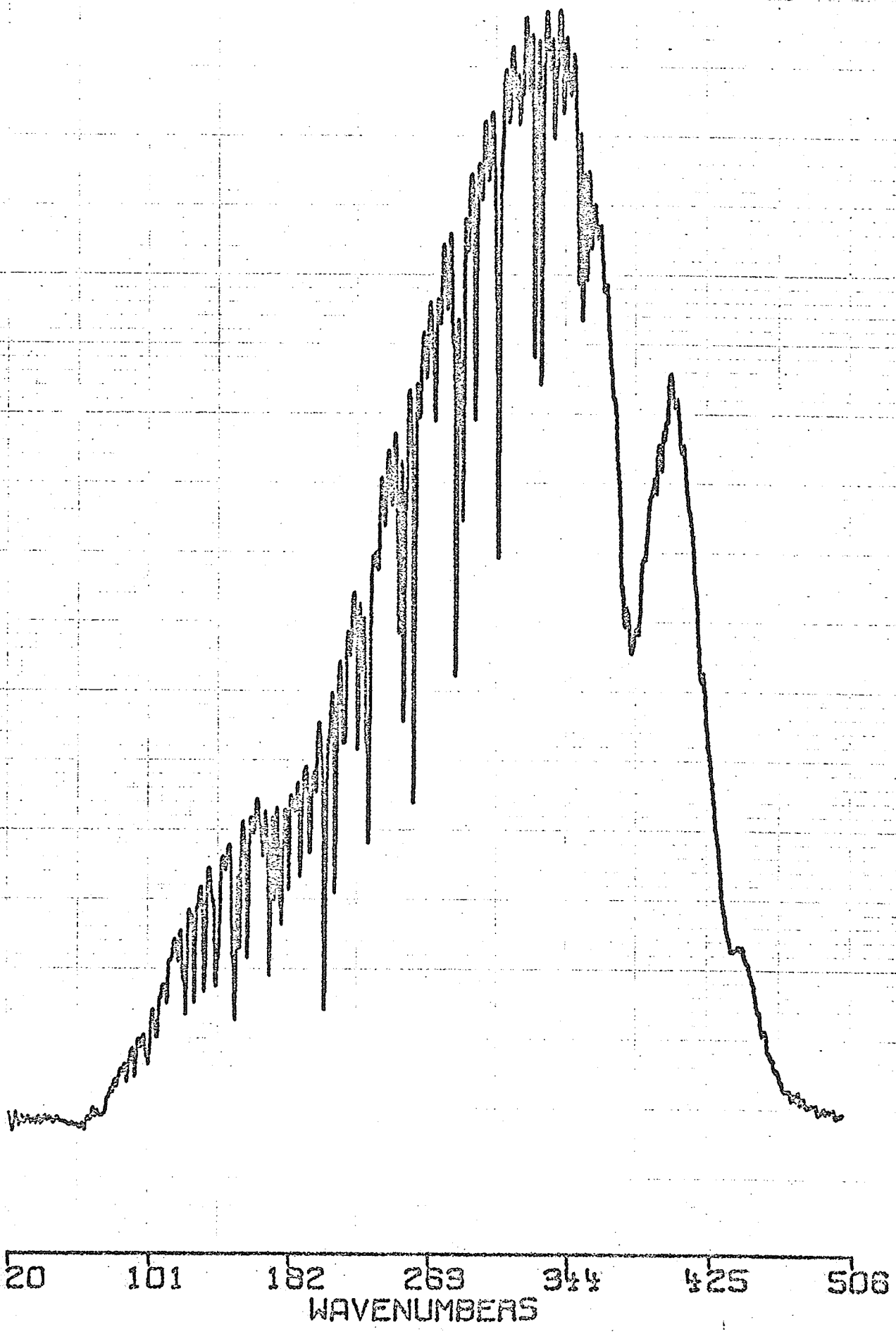

however, appeared in both the sample and background data and in most cases ratioed out completely in the final absorbance spectra.

Figure 11a is a typical high density HD spectrum. Note the sharp features at 178, 265 and 351 cm^{-1} corresponding to the R(1), R(2) and R(3) lines, shown in more detail in figures 11b-d. Evidence for the R(0) lines near 90 cm^{-1} and the R(4) line near 440 cm^{-1} is visible but neither are sufficiently distinct to warrant analysis. The general upward trend of the baseline towards the right-hand-side is caused by the collision-induced rotational spectrum of HD.

The area beneath the R(1), R(2) and R(3) lines, with the collision-induced component subtracted off, was found for each spectrum. These values are given in the following table (Table 2)

FIGURE 11a

The high pressure rotational spectrum of HD is given. The absorption peaks at 90, 178, 265, 351 and 435 cm^{-1} correspond to the R(0) through R(4) lines respectively.

FIGURE 11a THE HIGH PRESSURE ROTATIONAL SPECTRUM OF HD

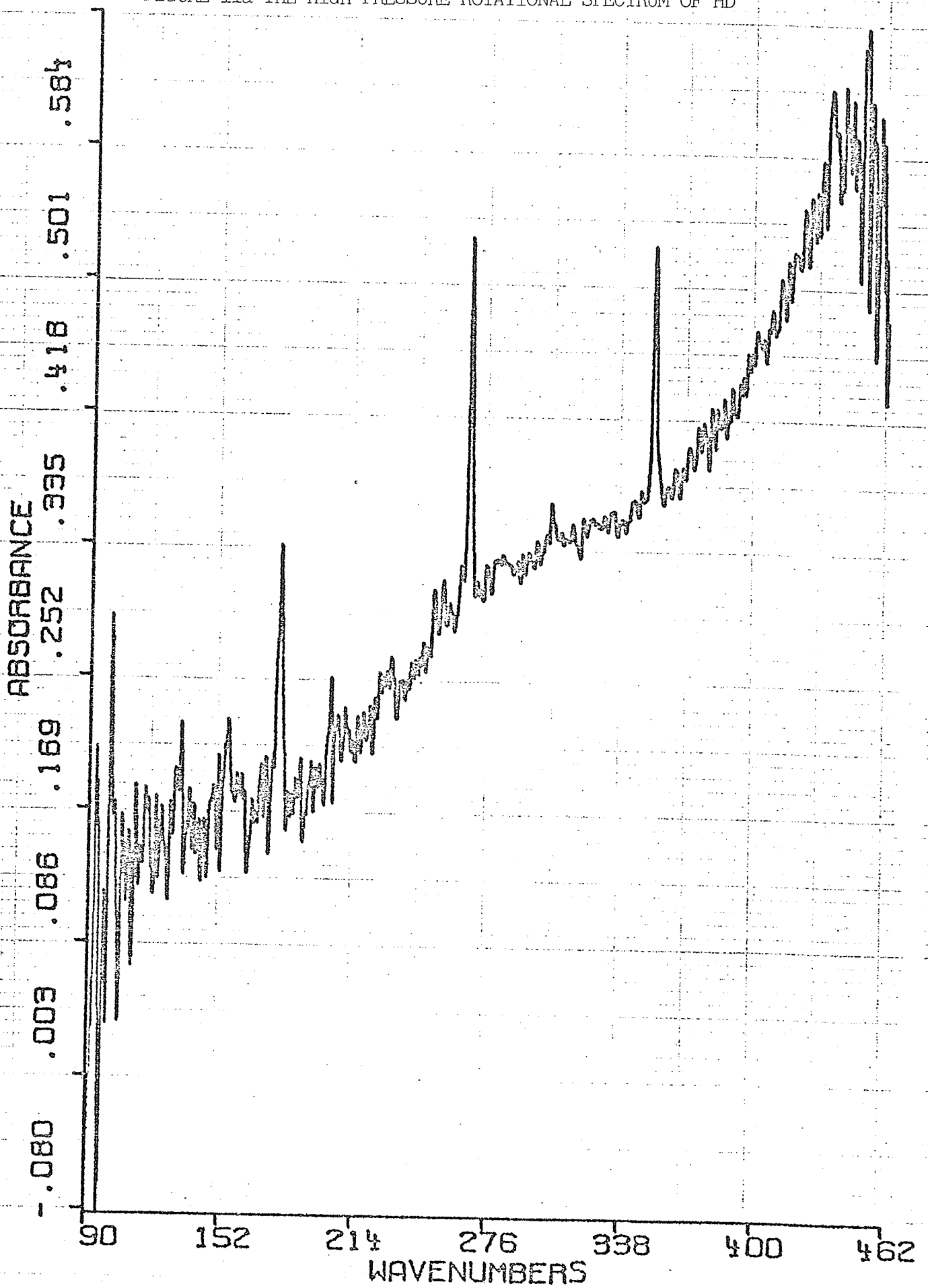

FIGURE 11b

This shows the R(1) line of HD at 56.3 Amagat.

Water lines are evident by the unusual lineshape.

FIGURE 11b THE R(1) LINE OF HD

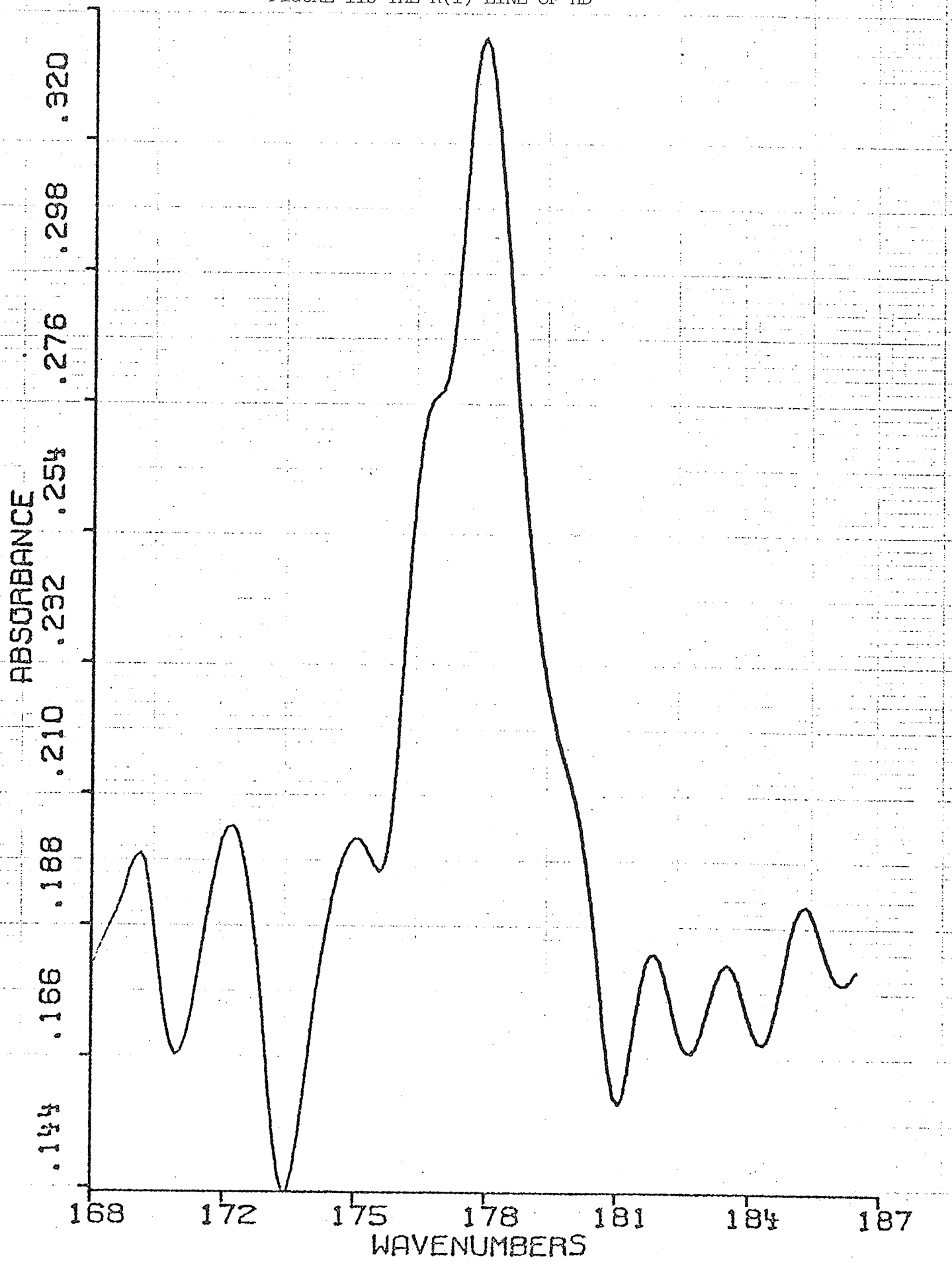

FIGURE 11c

This shows the R(2) line of HD at 56.3 Amagat. It is much more symmetric than the R(1) line because of the lack of water lines in this region.

FIGURE 11c THE R(2) LINE OF HD

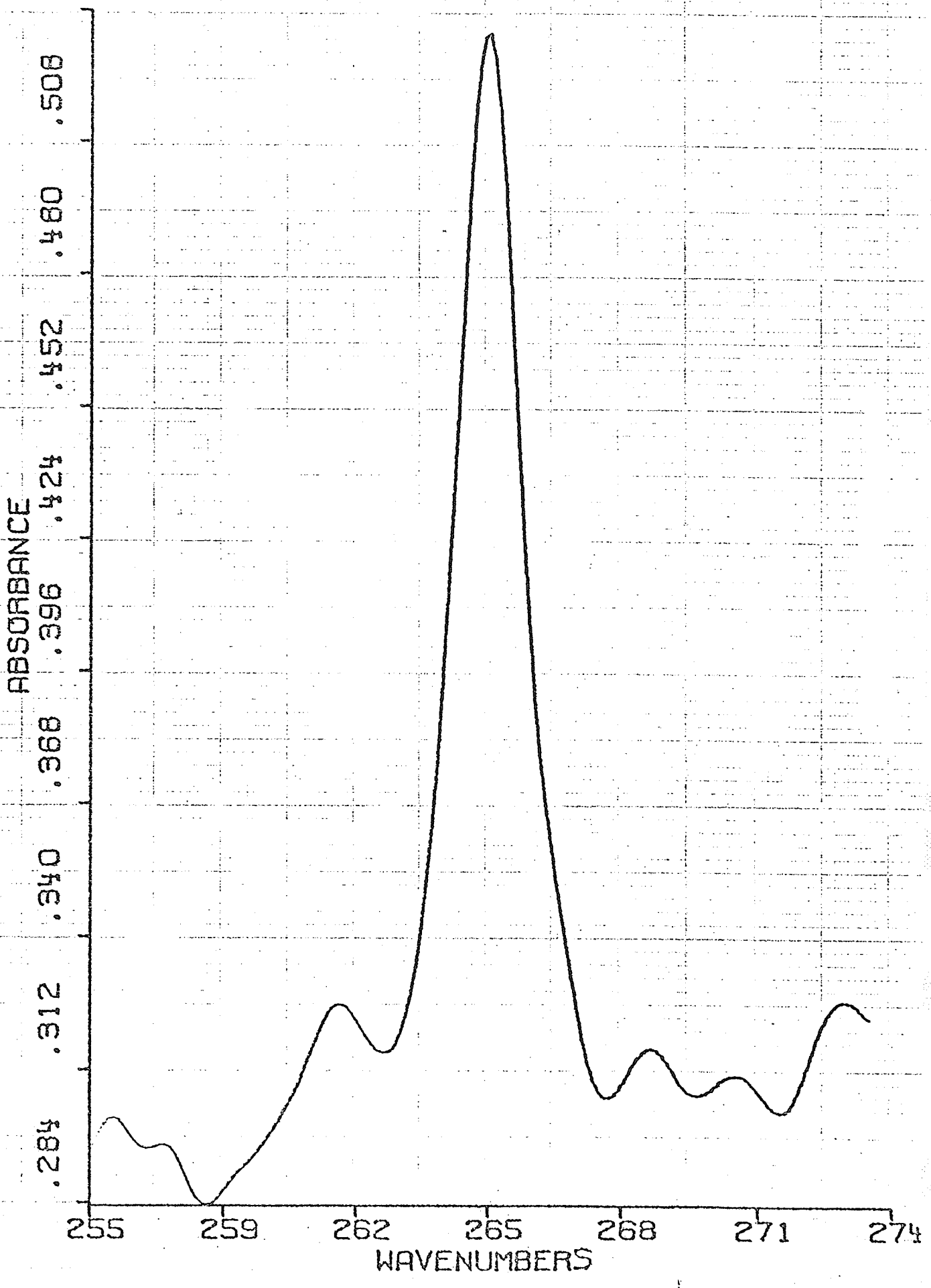

FIGURE 11d

This shows the R(3) line of HD at 56.3 Amagat. The apparent "tail" on the high energy side is caused by a superposition of water lines.

FIGURE 11d THE R(3) LINE OF HD

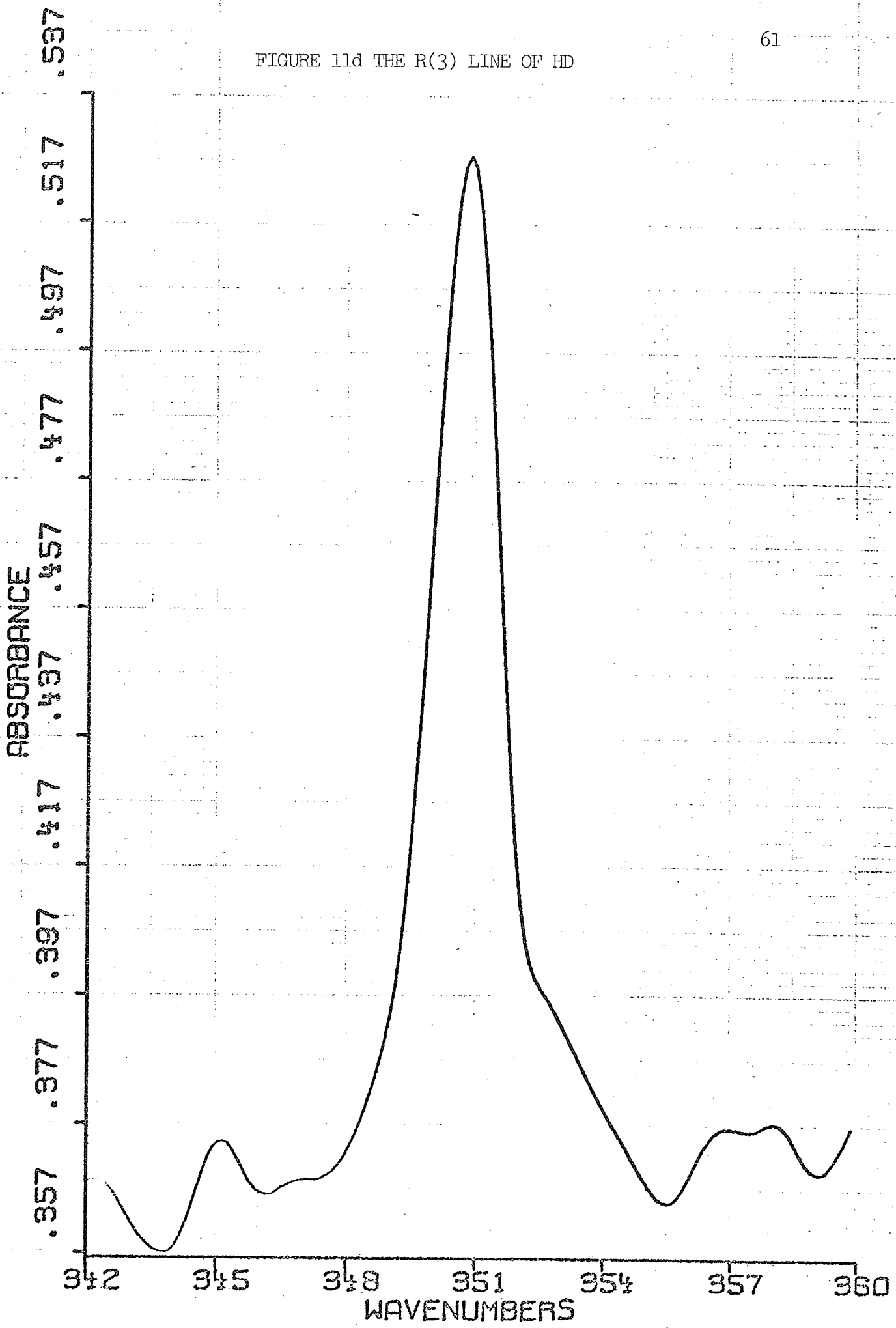

TABLE 2. INTEGRATED ABSORPTION VS. DENSITY

RUN A:

ρ(Amagat)	INTEGRATED INTENSITY (x 10^{-5} $Amagat^{-1}$ cm^{-1})		
	R(1)	R(2)	R(3)
7.2	26.1 ± 2.6	21.5 ± 1.8	15.4 ± 1.4
13.3	31.5 ± 2.8	23.3 ± 2.0	19.4 ± 1.6
19.4	23.8 ± 2.3	20.6 ± 1.7	18.2 ± 1.3
25.5	18.6 ± 1.9	17.4 ± 1.6	13.0 ± 1.2
31.6	13.2 ± 1.4	18.0 ± 1.6	13.0 ± 1.0
37.7	21.6 ± 1.9	18.9 ± 1.6	13.4 ± 1.0
43.8	19.1 ± 1.7	20.1 ± 1.7	16.1 ± 1.1
49.9	14.4 ± 1.3	16.4 ± 1.5	11.8 ± 1.0
56.3	16.2 ± 1.9	15.9 ± 1.5	10.5 ± .9
60.3	10.1 ± 1.1	14.4 ± 1.4	10.3 ± .8

RUN B:

4.4	- - -	27.5	14.7
9.0	32.8	18.6	17.9
12.0	24.7	17.5	15.1
15.1	23.3	24.9	17.5
18.1	30.9	28.5	24.3
21.1	24.8	17.5	9.9
24.2	15.1	13.8	12.1
25.7	14.5	17.6	15.2
27.2	28.2	20.4	14.2
28.8	12.9	21.2	12.3
30.3	27.5	19.0	12.7

CHAPTER 5

ANALYSIS OF DATA

From (2.22) we write

$$|p_{if}| = \left[\frac{1}{c_{if}} \frac{2.303}{\rho \ell} \int X_{if} \, d\omega \right]^{\frac{1}{2}}$$

Here $\int X_{if} \, d\omega$ is the area under an absorption line (on a Nicolet plotted spectrum) ρ is the density in Amagat, ℓ is the pathlength in cm, and C_{if} is a constant for each line, given by the following expression.

$$c_{if} = \omega_{if} \frac{8\pi^3 N_o}{3hcQ} \left[e^{-E_i/KT} - e^{-E_f/KT} \right] (J_i+1)$$

The values of C_{if} were calculated using T = 295° K, ω_{if} = 178, 265 and 351 cm^{-1} for the R(1), R(2) and R(3) lines respectively [8].

For a rigid rotator, in the ground vibrational state, the energy levels are given by

$$E(J) = B_v(J)(J+1)$$

The value of B_v used was 44.659 [13]. The constants C_{if} were found to be in excellent agreement with previous values [8], and are given in the following table.

TABLE 3. ANALYSIS CONSTANTS

J	(cm^{-1})	C ($Debye^{-2}$ $Amagat^{-1}$)
1	178	315
2	265	359
3	351	190

To convert pressure measurements to Amagat density, we used a first order virial expansion [33]

$$PV = RT\,[1 + B/V)$$

A value of B for HD was not available in the correct temperature region. Instead we approximated it by the value of B for H_2 at 295°C. Solving this equation for V gives:

$$V(T) = RT/P\,[1 + BP]$$

B was found to be 14.5 cm^3 $mole^{-1}$ [32]. Denoting the volume of 1 mole of gas at 1 atmosphere at 0°C by V_o, we have

$$\rho_{AMAGAT} = \frac{1}{V(T)} \Big/ \frac{1}{V_o}$$

$$= \frac{V_o}{V(295)}$$

Substituting the equation for V(T) into this gives us the approximate relation used to convert pressure in atmospheres to Amagat density:

$$\rho_{AMAGAT} \approx .927\ P_{ATMOSPHERES}.$$

There were two main difficulties encountered in attempting to measure the area under an HD absorption peak. It was impossible to

FIGURES 12a-c

There are plots of integrated absorption vs. density for the R(1), R(2) and R(3) lines of HD, run A. The straight lines through the data were obtained by a weighted least squares fit to the data, as justified by equation 3.17.

FIGURE 12a

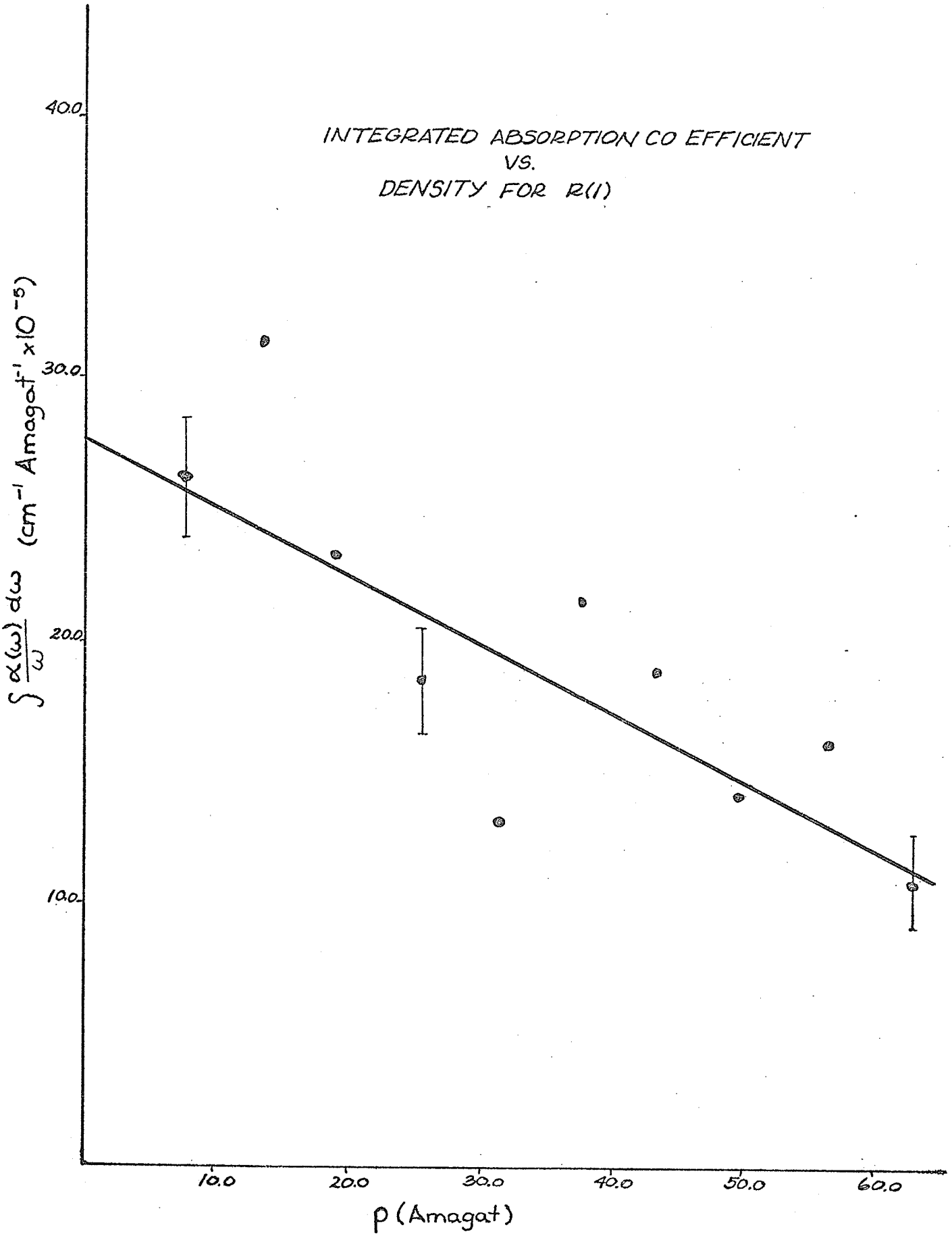
INTEGRATED ABSORPTION CO EFFICIENT
VS.
DENSITY FOR R(1)
$\int \frac{\alpha(\omega)}{\omega} d\omega$ (cm^{-1} Amagat^{-1} x10^{-5})
40.0
30.0
20.0
10.0
10.0
20.0
30.0
40.0
50.0
60.0
ρ (Amagat)

FIGURE 12b

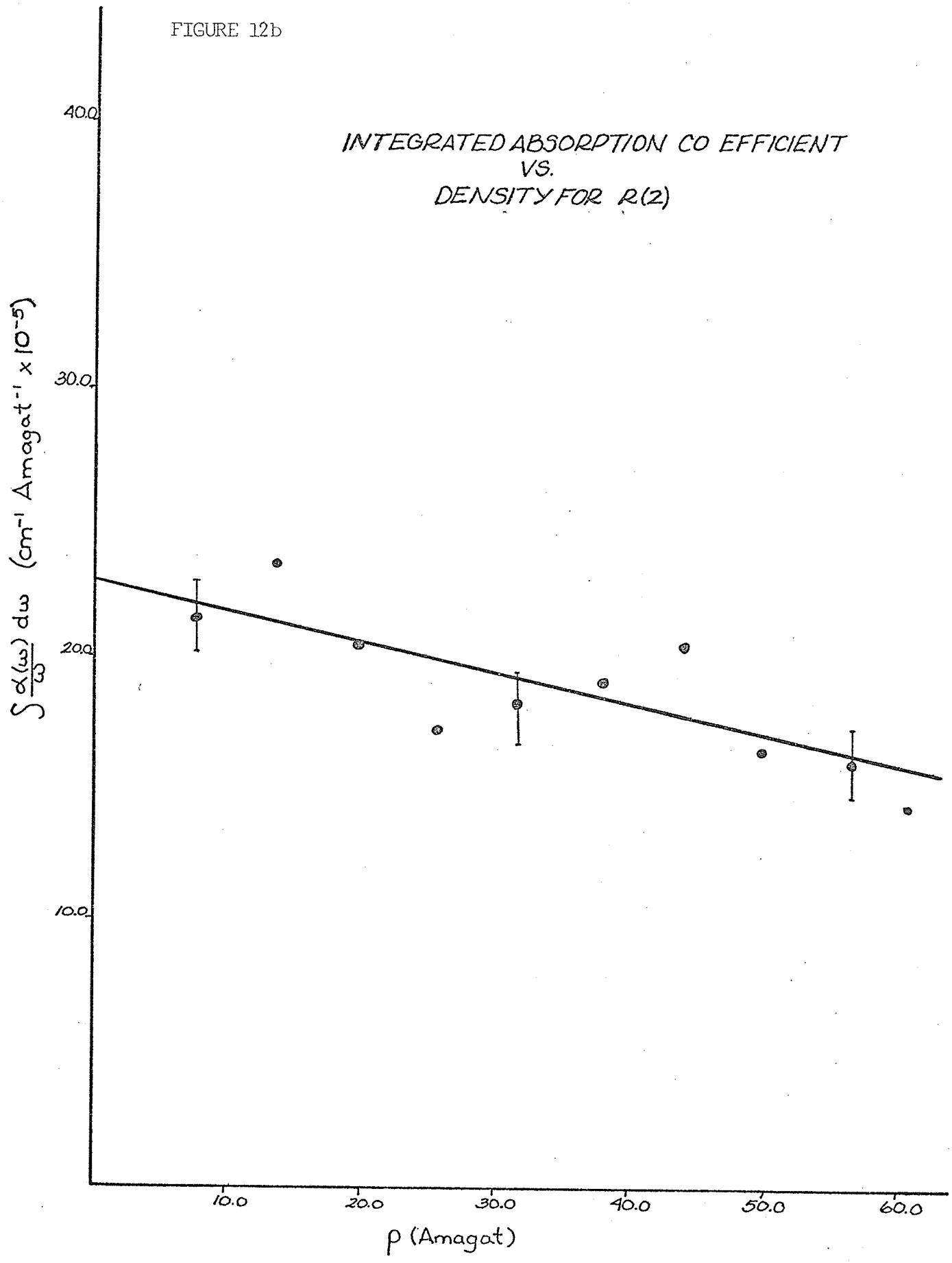
INTEGRATED ABSORPTION CO EFFICIENT
VS.
DENSITY FOR R(2)
40.0
30.0
20.0
10.0
$\int \frac{\alpha(\omega)}{\omega} d\omega$ (cm^{-1} Amagat^{-1} x 10^{-5})
10.0
20.0
30.0
40.0
50.0
60.0
ρ (Amagat)

FIGURE 12c

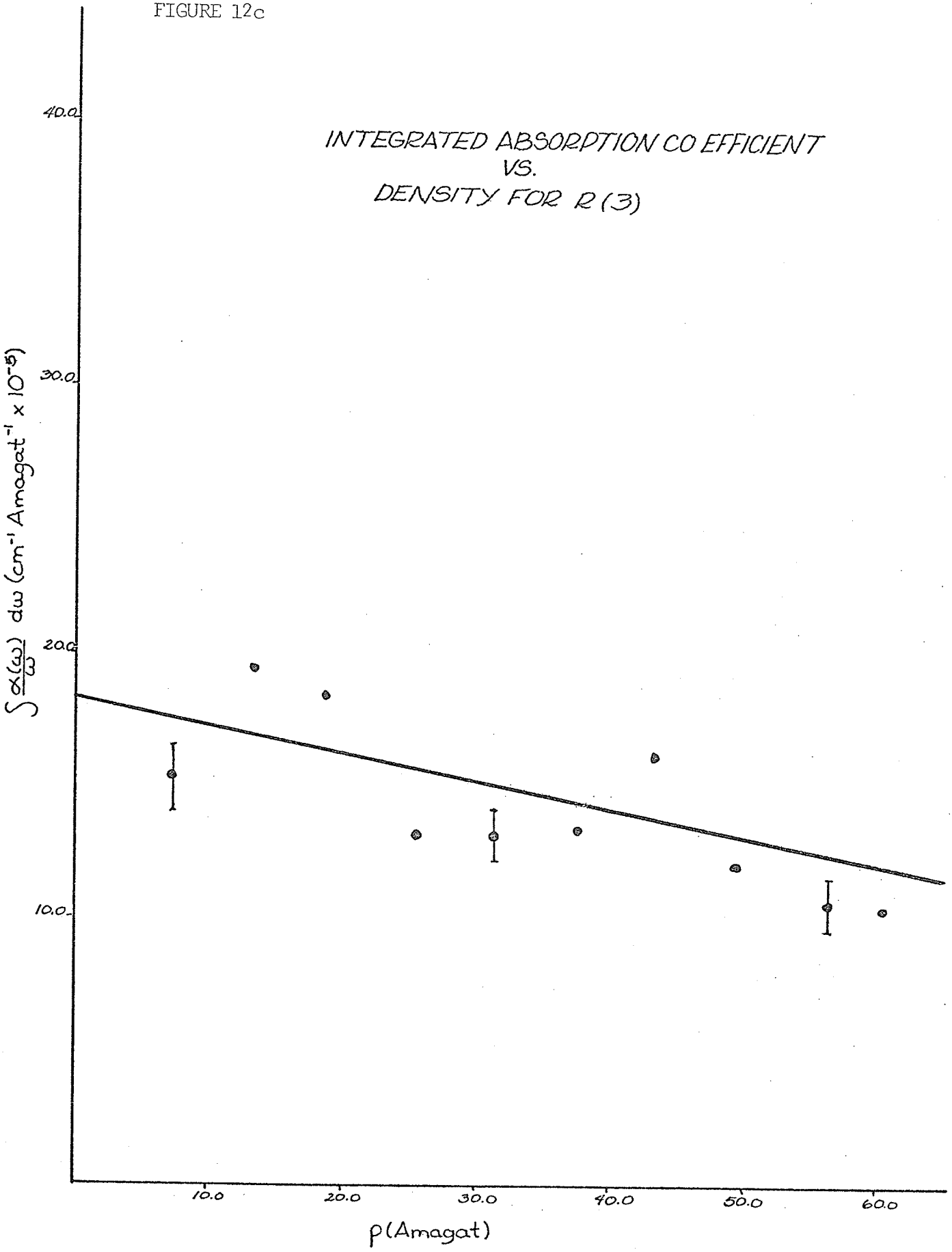
INTEGRATED ABSORPTION CO EFFICIENT
VS.
DENSITY FOR R(3)
40.0
30.0
20.0
10.0
$\int \frac{\alpha(\omega)}{\omega} d\omega$ (cm^{-1} Amagat^{-1} x 10^{-5})
10.0
20.0
30.0
40.0
50.0
60.0
ρ(Amagat)

completely purge the equipment of water vapor, only to reduce it to a minimum level. Ratioing of the sample to the background did not exactly cancel the water lines. Consequently there was a superposition of small intensity water lines and HD lines in most cases. The 265 cm^{-1} line was the cleanest as it does not lie near a water line. The 178 cm^{-1} and 351 cm^{-1} lines were often obscured by water and thus crude curve fitting techniques had to be employed to calculate the integrated absorption coefficient.

The second and more bothersome difficulty was determining the baseline. Although each run encompassed several thousand scans to maximize the signal-to-noise ratio, the baseline on the low pressure runs was somewhat difficult to locate. Consequently, an error estimate to 10% was used in finding the baseline.

For each absorption line (R(1), R(2), R(3)) we calculated the dipole strength over a pressure range of ~5 - 60 Amagat. These results were plotted on integrated intensity vs. density graphs and are given in figures 12a-c. With equation (3.17) as justification, we used a weighted least squares fit [24] of the data to straight lines. The relative weighting of the points was determined by the error bars associated with each point. We extrapolated these graphs back to "zero density" to yield a value of $|\mu_o|$, the permanent dipole moment of HD in the ground vibrational state. From the slope of the line and the intercept we calculated the intracollisional interference parameter "a". (see Table 4)

A second set of data taken earlier, Run B, is given in figures 13a-c. This data exhibits much larger scatter and as a

FIGURES 13a-c

These are plots of integrated absorption vs. density for the R(1), R(2) and R(3) lines of HD, run B. The straight lines were obtained by a least squares fit of the data, as justified by equation (3.17). The large error bars are due to increased water content in the sample gas.

FIGURE 13a

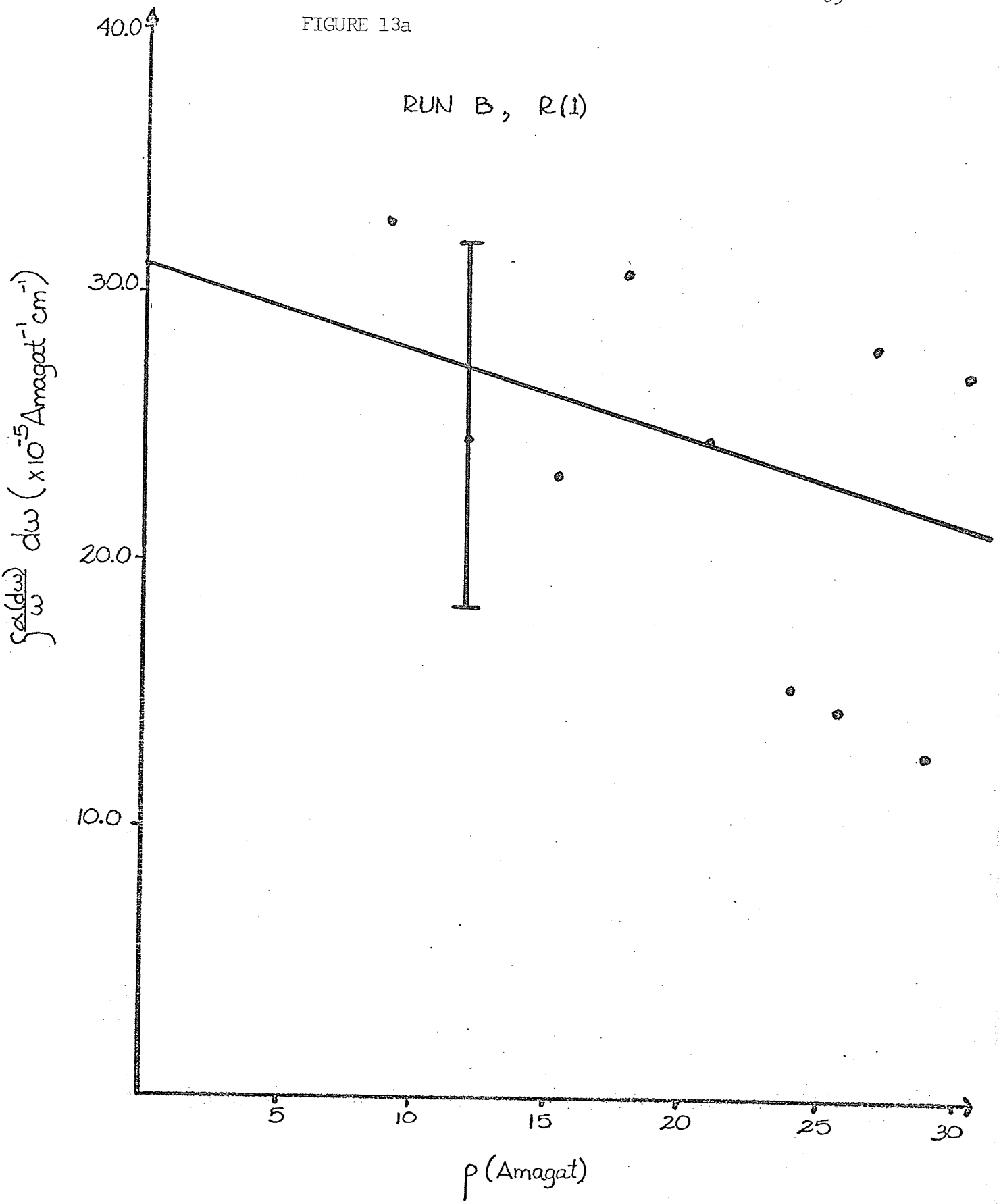
RUN B, R(1)
40.0
30.0
20.0
10.0
$\int \frac{\alpha(d\omega)}{\omega} d\omega$ ($\times 10^{-5}$ Amagat^{-1} cm^{-1})
5
10
15
20
25
30
p (Amagat)

FIGURE 13b

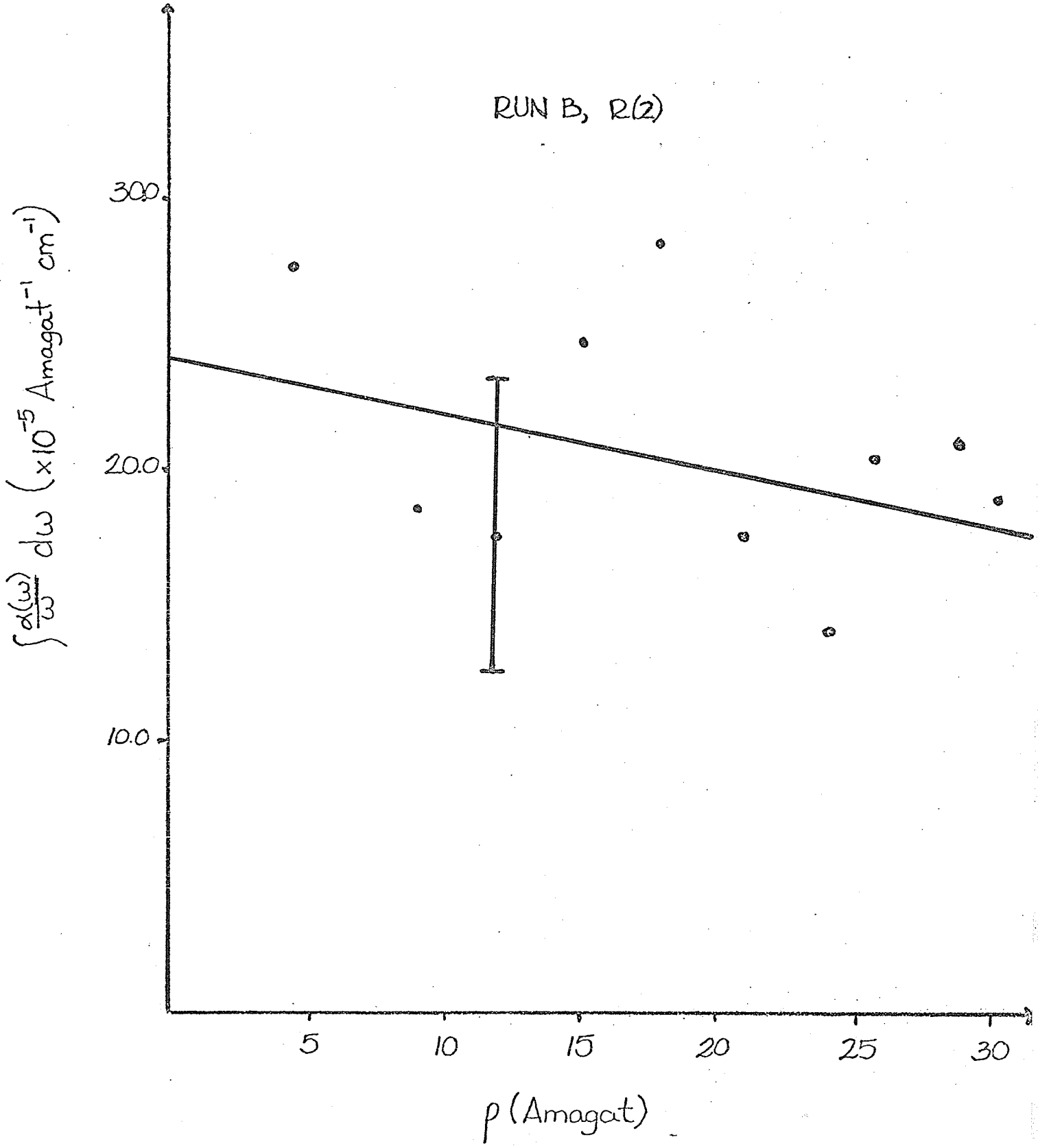
RUN B, R(2)
30.0
20.0
10.0
$\int \frac{\alpha(\omega)}{\omega} d\omega$ ($\times 10^{-5}$ Amagat^{-1} cm^{-1})
5
10
15
20
25
30
ρ (Amagat)

FIGURE 13c

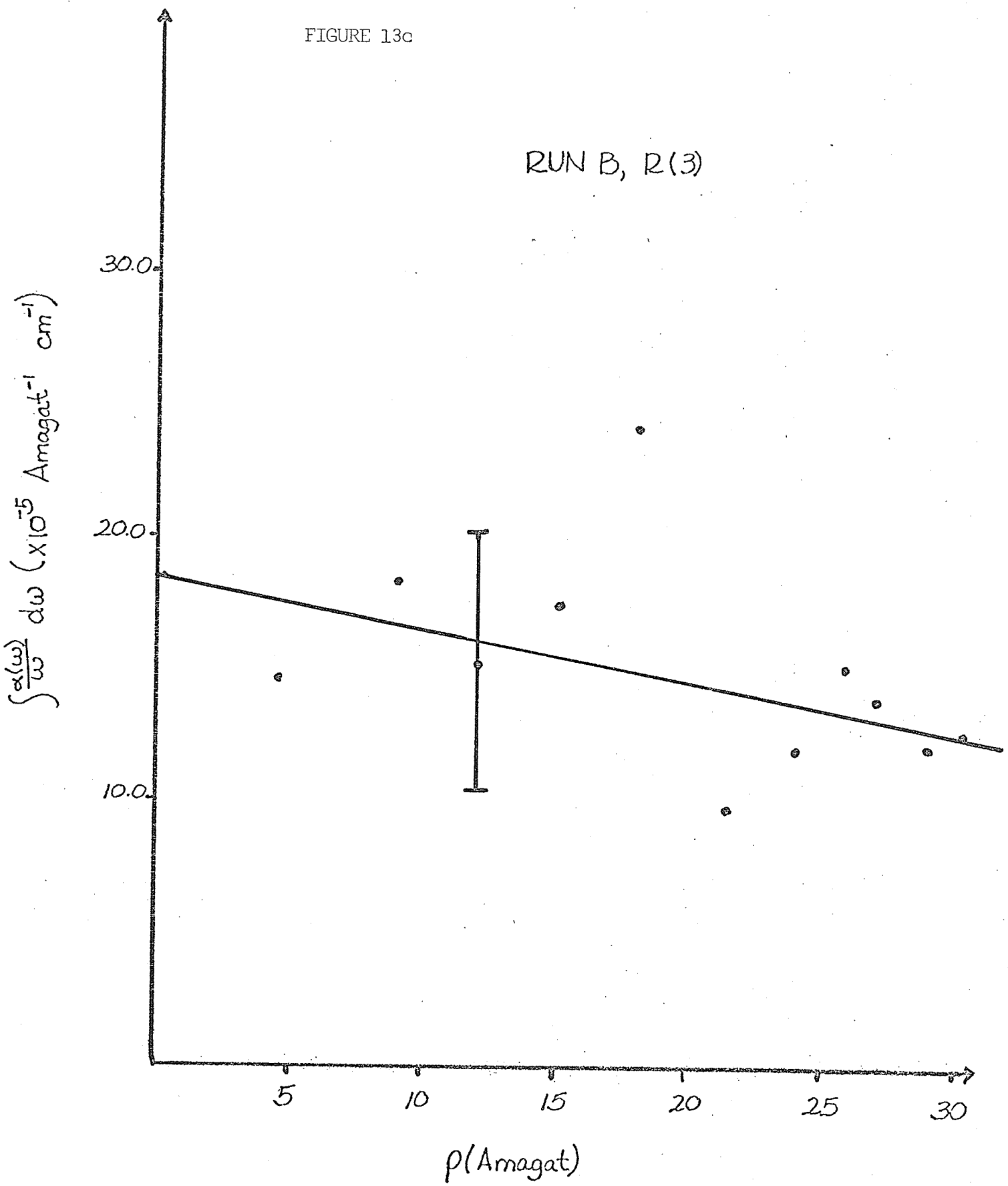
RUN B, R(3)
30.0
20.0
10.0
$\int \frac{\alpha(\omega)}{\omega} d\omega$ ($\times 10^{-5}$ Amagat^{-1} cm^{-1})
5
10
15
20
25
30
ρ(Amagat)

consequence, much larger error bars. This is due to the increased water content in the sample and hence even more difficulty in analysis. This data has not been included to further define the quantities of "μ_o" and "a", but rather to demonstrate the reproducibility of our results. (see Table 4)

TABLE 4

EXPERIMENTAL RESULTS FOR $|\mu_o|$ AND "a" AS FUNCTIONS OF J

RUN A

	DATA	USING WEIGHTED LEAST SQUARES LINEAR REGRESSION
LINE	$\|\mu_o\| \times 10^{-4}$ D	$a \times 10^{-3}$ Amagat^{-1}
R(1)	9.36 ± .27	-9.50 ± .49
R(2)	8.00 ± .19	-5.50 ± 1.30
R(3)	9.79 ± .24	-6.90 ± 1.14

RUN B

	DATA	USING BEST FIT LEAST SQUARES LINEAR REGRESSION
	$\|\mu_o\| \times 10^{-4}$ D	$a \times 10^{-3}$ Amagat^{-1}
R(1)	9.86	-9.40
R(2)	8.22	-7.98
R(3)	9.83	-10.69

CHAPTER 6

DISCUSSION

The three lines analysed all exhibited a negative slope with relatively consistent intercepts. Although ab initio calculations [1], [3] indicate a very slight J-dependence for μ_o, we noticed a pronounced variation of μ_o with J. This could be attributable to water uncompensated for in the R(1) and R(3) lines but the consistency of the two data sets A and B tends to indicate otherwise.

Similarly the value of "a" is somewhat J-dependent according to our results. Tipping and Poll neglected the effects of rotational level mixing by anisotropic intermolecular forces in their calculations. This effect would be most pronounced at the lower energy (and thus J) levels and might be expected to alter their value for R(0) and R(1). It would be less effective at higher energy (J) levels. Thus the theory is more applicable to the R(2), R(3) and higher lines. The fact that our measured value of $|a|$ for R(2) and R(3) lies very close to their calculated value of $|a|$ and that our value for R(1) is larger than their predicted value lends credibility to their theory.

If the data is extrapolated to a density of 100 Amagat, the dipole moments for each of the R(1), R(2) and R(3) lines would be between 5.0 and 6.0 x 10^{-4} D. As these are the values obtained by Trefler and Gush, it is obvious that the difference between theoretical values and their values for the dipole moment is attributable to

intracollisional interference.

Because the slopes of the integrated absorption vs. density graphs are negative, the signs of the allowed and induced moments are opposite. Adopting the convention of Wolniewicz and assigning a negative sign to the allowed ground vibrational dipole moment, we therefore assign a positive sign to the induced dipole moment. This is agreement with measurements by McKellar [9] on the fundamental band.

Another observed effect was the "Fano-lineshape" [35] at mid-densities. (see Figure 14) This skewness was only apparent on the R(2) line at densities between 20 and 40 Amagat, quite possibly because these lines were the most water-free.

This lineshape was predicted by Tipping and Poll because the profiles of the permanent dipole term and the intracollisional interference term are different. The permant dipole moment gives rise to the usual Lorentzian lineshape while the interference term yields an anomalous dispersion profile. The sum of these is then a Fano-lineshape.

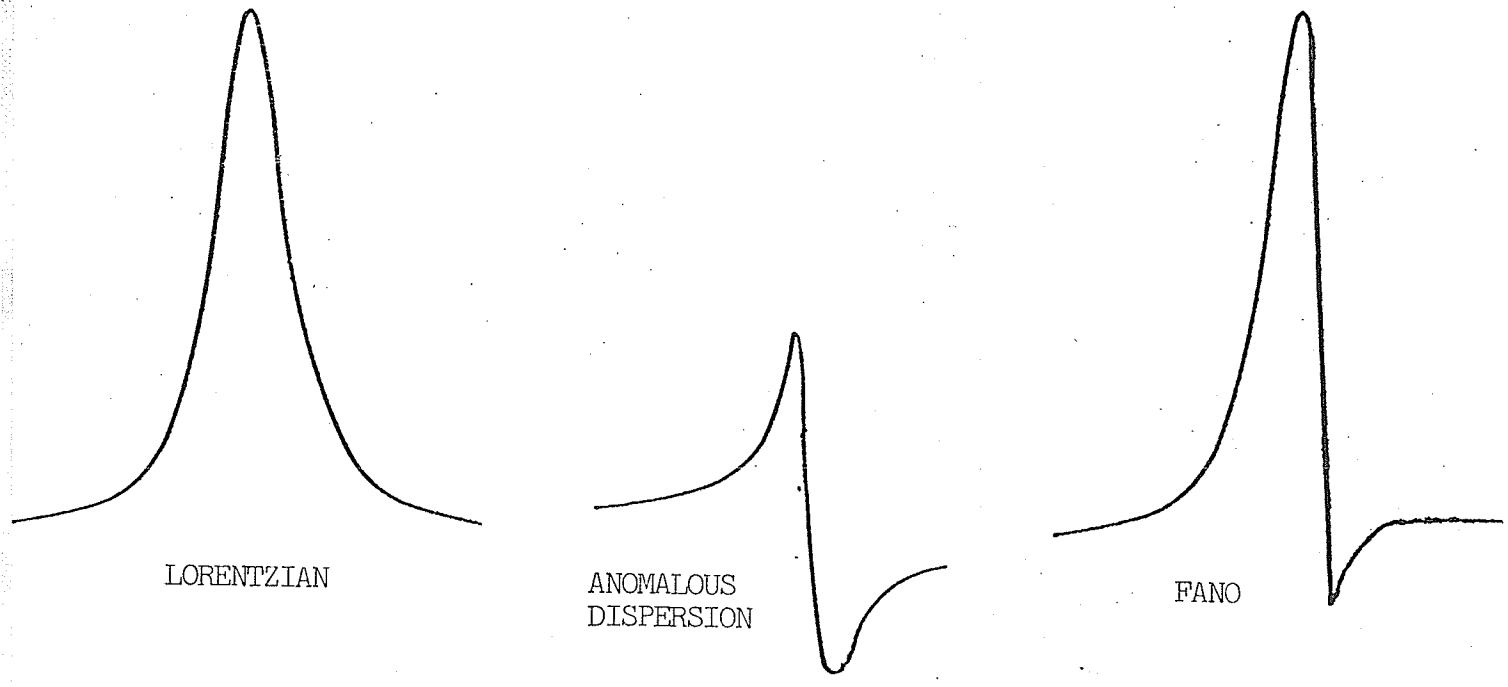

From [26] the total absorption

coefficient per unit wavelength per unit density is

$$\int \frac{\alpha(\omega)}{\omega} d\omega = \frac{N_o}{3hc} P(J) (J+1) (p^A_{JJ'})^2 \cdot \left[\frac{\Gamma'_{JJ'}}{(\tfrac{1}{2} \Gamma'_{JJ'})^2 + (\omega - \omega_{J'J})^2} [1 + 2\rho N_o \Delta' I] + \frac{4(\omega - \omega_{JJ'})}{(\tfrac{1}{2} \Gamma'_{JJ'})^2 + (\omega - \omega_{JJ'})^2} (\rho N_o \Delta''_{JJ'} I) \right]$$

$P(J)$ - is a Boltzmann function satisfying $\sum_J (2J + 1) P(J) = 1$

$\Gamma_{JJ'}$ - is the full width at half maximum

$\omega_{JJ'}$ - is the peak frequency

Δ'' and Δ' - are the fitting parameters

and $I = 4\pi \int_o^\infty p^I_{JJ'}(R)\, g(R)\, R^2\, dR$ as defined by eqn. 3.10.

The presence of the Fano-lineshape in our absorption spectra lends credibility to the theory of intracollisional interference.

If the two sets of data for the R(2) line are combined (see Figure 15), then a distinct oscillation in the integrated intensity vs. density graph is observed. This trend may be accounted for by the error bars in each run and as there has been no theoretical basis for this phenomenon presented as yet, we assumed the oscillations to be random fluctuations about the linear relationship. Any oscillations in the R(1) or R(3) lines are masked by the scatter in the data.

FIGURE 14

THE FANO-SHAPE OF THE R(2) LINE IN HD AT 31.6 AMAGAT

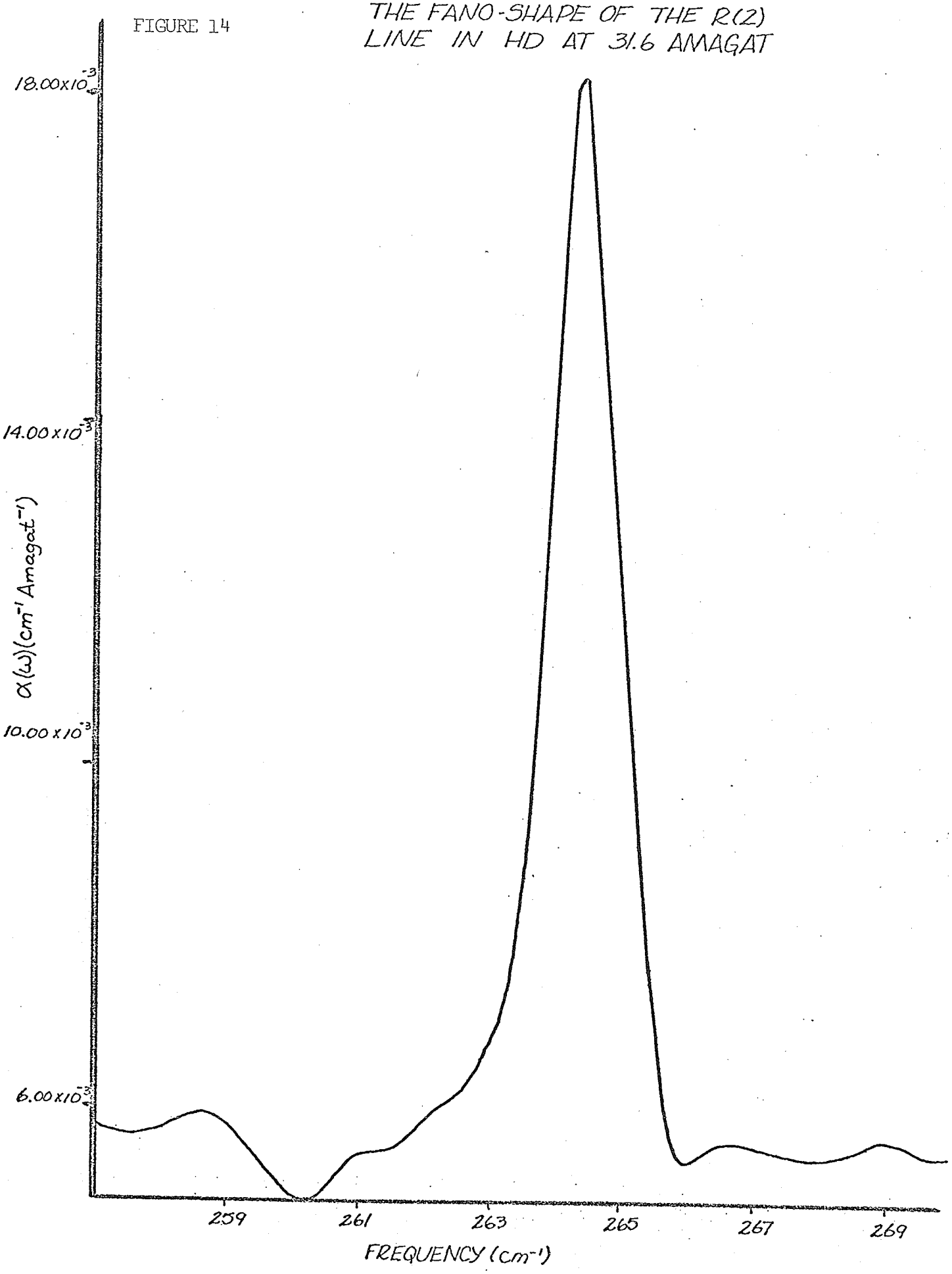

FIGURE 15

This is a plot of the combined (RUN A + RUN B) R(2) integrated absorption vs. density. The oscillation in the data may be of theoretical importance or simply random fluctuations as we have assumed.

FIGURE 15

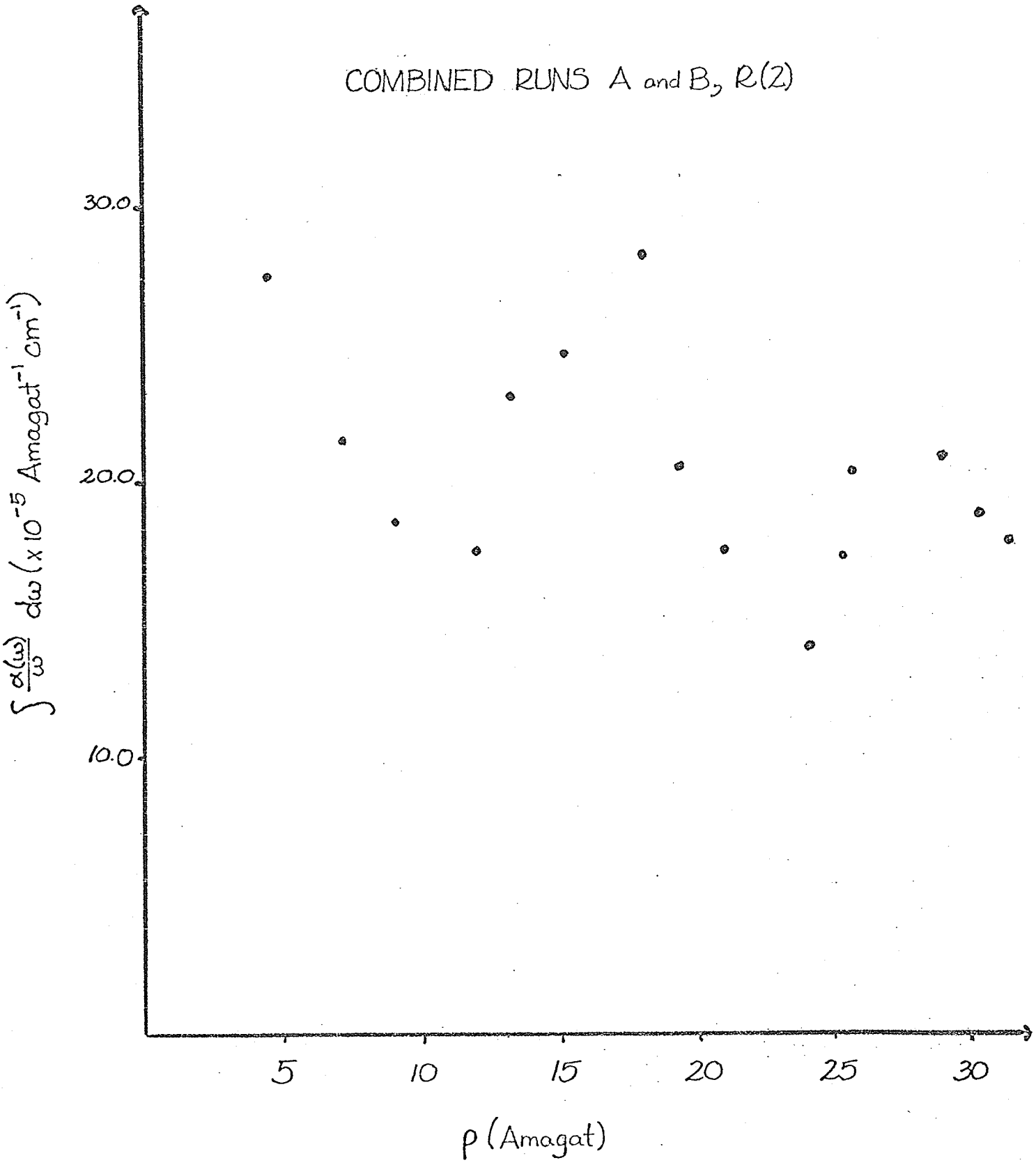
COMBINED RUNS A and B, R(2)
30.0
20.0
10.0
$\int \frac{\alpha(\omega)}{\omega} d\omega$ ($\times 10^{-5}$ Amagat^{-1} cm^{-1})
5
10
15
20
25
30
ρ (Amagat)

CHAPTER 7

CONCLUSIONS

A comparison between the transition moments calculated by Wolniewicz [1], Ford and Browne [3],and found experimentally by Gush [8] and the present work is given in the following table.

TABLE 5. THE PERMANENT DIPOLE MOMENT OF HD (in 10^{-4} D)

	WOLNIEWICZ	FORD & BROWNE	|GUSH†|	|PRESENT WORK†|
R(0)	-8.36	-8.31	5.42	- - -
R(1)	-8.38	-8.30	5.52	9.4 ± .3
R(2)	-8.39	-8.28	6.18	8.0 ± .2
R(3)	-8.41	-8.26	6.41	9.8 ± .4

The ground vibrational permanent dipole moment appears to be J-dependent and ranges from -8.0 ± .2 to -9.8 ± .4 x 10^{-4} D. The errors quoted are those given by a least squares fit of the data to a straight line, where the weighting of each point is relative to the magnitude of the error bar associated with it. These values are in excellent agreement with ab initio calculations [1], [3], [4] which indicate a value of approximately -8.4 x 10^{-4} D.

The intracollisional interference parameter "a" was found to be J-dependent, ranging from -5.5 ± 1.3 to -9.6 ± .5 x 10^{-3} Amagat^{-1}.

---

† experimental results

These results are consistent with the expectation value of $|a| = 5.4 \times 10^{-3}$ Amagat^{-1}, as predicted by [1]. The negative sign associate with "a" indicates that the sign of the induced moment is opposite to that of the permanent dipole moment, i.e. $\mu_o^I > 0$.

Further experimentation is in progress to clarify the other observed effects. Mixtures of HD with heavy, inert, perturbing gases (i.e. Krypton and Xenon) would allow us to alter the induced moment, keeping the permanent moment the same. This would change the value of the intracollisional interference parameter, thereby enabling us to further test the theory of intracollisional interference already observed in the fundamental band by McKellar [9].

Low temperatures would change the stimulated emission term $(e^{-E_i/KT} - e^{-E_i/KT})$ in equation (2.1). This would allow us to calculate the permanent dipole moment of HD under different conditions to check the validity of our results. Also these experiments would allow us to observe the evolution of the Fano-lineshape.

The oscillations which may be present in the combined R(2) data (Figure 15) could be confirmed by using a finer mesh of densities with more attention paid to eliminating water vapor from the system.

Low density experiments may enable us to reconcile with

theory the apparent J-dependence of the ground vibrational permanent dipole moment of HD. i.e at low densities, the relationship between $\int \frac{\alpha(\omega)}{\omega} d\omega$ and ρ may become strongly non-linear, with the intercepts of all lines (R(1), R(2) and R(3))being equal. This possibility is being studied at present [28] although we are unaware of any definitive results as yet.

REFERENCES

[1] Wolniewicz L., Can. Jour. Phys. 54, 672 (1976).

[2] Wolniewicz L., Can. Jour. Phys. 53, 1207 (1975).

[3] Ford L. and Browne J., Phys. Rev. A 16 1992 (1977).

[4] Bunker P., Jour. Mol. Spec. 46, 119 (1973).

[5] Kolos W., Wolniewicz L., Rev. Mod. Phys. 35, 473 (1963).

[6] Kolos W., Wolniewicz L., Jour. Chem. Phys. 45, 944 (1966).

[7] Tipping R.H., Poll J.D., and McKellar A.R.W., Can. Jour. Phys. 56, 75 (1978).

[8] Trefler M. and Gush H. P., Phys. Rev. Lett. 20, 703 (1968).

[9] McKellar A.R.W., Can. Jour. Phys. 51, 389 (1973).

[10] Wick G. C., Atti R. Accad. Naz. Lincei, Mem. Cl. Sci. Fis. Mat. Nat. 21 708 (1935).

[11] Merzbacher E., Quantum Mechanics, John Wiley and Sons, New York, Chapter 17 (1961).

[12] Böhn A, Quantum Mechanics, Springer-Verlag, New York, Chapter 2 (1979).

[13] Herzberg G., Spectra of Diatomic Molecules, D. Van Nostrand Co., New York, p. 532 (1959).

[14] Ford L. and Browne J., Phys. Rev. A7 418 (1973).

[15] Wu T.Y., Can. Jour. Phys. 30, 291 (1952).

[16] Anderson E., Modern Physics and Quantum Mechanics, W. B. Saunders Company, London (1971).

[17] Herzberg G., Nature 166, 563 (1950).

[18] Blinder S.M., Jour. Chem. Phys. 32, 105 (1960).

[19] Blinder S.M., Jour. Chem. Phys. 35, 974 (1961).

[20] Rose M. E., Elementary Theory of Angular Momentum, John Wiley and Sons, New York, Chapter 4 (1966).

[21] Gasiorowicz S., The Structure of Matter, Addison-Wesley, London p. 355 (1979).

[22] Garbuny M., Optical Physics, Academic Press, New York, Chapter III (1965).

[23] Bohm A., Quantum Mechanics, Springer-Verlag, New York Chapter III (1979).

[24] Ibid, Chapter V

[25] Rose M. E., Elementary Theory of Angular Momentum, John Wiley and Sons, New York, Chapter V (1966).

[26] Herman R. M., Tipping R. H., and Poll J. D., Phys. Rev. A20, 2006 (1979).

[27] Poll J.D., Tipping R.H., Prasad R.D.G., and Reddy S. P., Phys. Rev. Lett. 36, 248 (1976).

[28] Poll J.D., private communication (1981).

[29] Nicolet Instrument Corp. Instruction Manual, Madison Wisconsin (1981).

[30] Horne R. K. and Birnbaum G., Infrared Physics 17, 173 (1977).

[31] Kiss Z.J., Gush H.P., and Welsh H.L., Can. Jour. Phys. 37, 362 (1959).

[32] Harries J.E., Jour. Op. Soc. Am. 69, 386 (1979).

[33] Dymond J.H. and Smith E.B., The Virial Coefficients of Gases, Clarendon Press, Oxford, p. 164 (1969).

[34] Bevington P.R., Data Reduction and Error Analysis for the Physical Sciences, McGraw-Hill, New York, Chapter VI (1969).

[35] Fano U., Phys. Rev. 124, 1866 (1961).